THERMAL AND PHOTOCATALYTIC DECOMPOSITION OF ORGANOPHOSPHONATES

FINAL PROGRESS REPORT

SUNITA SATYAPAL*, STEVEN SUIB, LIXIN CAO, TIMOTHY OBEE,
XIA TANG, ROBERT HALL

DECEMBER 5 1999

U.S. ARMY RESEARCH OFFICE

DAAH04-96-C-0067

UNITED TECHNOLOGIES RESEARCH CENTER

APPROVED FOR PUBLIC RELEASE;
DISTRIBUTION UNLIMITED.

REPORT DOCUMENTATION PAGE

Form Approved
OMB NO. 0704-0188

1. AGENCY USE ONLY (Leave Blank)	2. REPORT DATE December 1999	3. REPORT TYPE AND DATES COVERED Final Report

4. TITLE AND SUBTITLE

Thermal and Photocatalytic Decomposition of Organophosphonates

5. FUNDING NUMBERS

DAAH04-96-C-0067

6. AUTHOR(S)

Sunita Satyapal, Steven Suib, Lixin Cao, Timothy Obee, Xia Tang, Robert Hall

7. PERFORMING ORGANIZATION NAME(S) AND ADDRESS(ES)

United Technologies Research Corporation
Research Center
Silver Lane Hartford, CT 06108

8. PERFORMING ORGANIZATION REPORT NUMBER

9. SPONSORING / MONITORING AGENCY NAME(S) AND ADDRESS(ES)

U. S. Army Research Office
P.O. Box 12211
Research Triangle Park, NC 27709-2211

10. SPONSORING / MONITORING AGENCY REPORT NUMBER

ARO 35623.3-CH

11. SUPPLEMENTARY NOTES

The views, opinions and/or findings contained in this report are those of the author(s) and should not be construed as an official Department of the Army position, policy or decision, unless so designated by other documentation.

12 a. DISTRIBUTION / AVAILABILITY STATEMENT

Approved for public release; distribution unlimited.

12 b. DISTRIBUTION CODE

13. ABSTRACT (Maximum 200 words)

During the final year of this program, novel catalysts were developed and tested for the destruction of the CWA simulant, DMMP. The breakthrough result of over 100 hours of continuous operation at a nominal conversion of 99.9% was demonstrated, with no apparent poisoning of the catalyst. Products and spent catalysts were characterized using IC, FTIR, XPS, BET, and GC techniques and mechanistic pathways were postulated. In addition, a model was used to design a photocatalytic reactor for the destruction of DMMP on titania. A prototype reactor was constructed and the conversion efficiency was measured to be in reasonable agreement with the model's prediction. Reactor size requirements were calculated for optimum destruction of DMMP.

14. SUBJECT TERMS

15. NUMBER OF PAGES

16. PRICE CODE

17. SECURITY CLASSIFICATION OR REPORT	18. SECURITY CLASSIFICATION ON THIS PAGE	19. SECURITY CLASSIFICATION OF ABSTRACT	20. LIMITATION OF ABSTRACT
UNCLASSIFIED	UNCLASSIFIED	UNCLASSIFIED	UL

NSN 7540-01-280-5500

Standard Form 298 (Rev.2-89)
Prescribed by ANSI Std. 239-18
298-102

TABLE OF CONTENTS

FINAL REPORT (Sept.1998-Sept. 1999)

(1) LIST OF MANUSCRIPTS submitted or published under ARO sponsorship during this reporting period, INCLUDING JOURNAL REFERENCES:

"Thermocatalytic Oxidation of Dimethyl Methylphosphonate on Supported Metal Oxides", Lixin Cao, Scott R. Segal, Steven L. Suib, Xia Tang, Sunita Satyapal, manuscript to be submitted

"Thermocatalytic Destruction of Dimethyl Methylphosphonate on Activated Carbon", Lixin Cao, Steven L. Suib, Xia Tang and Sunita Satyapal, manuscript to be submitted

"Gas-Phase Photocatalytic Decomposition of DMMP on TiO_2 and Reactor Design Model Validation", Sunita Satyapal, Timothy N. Obee, and Robert J. Hall, manuscript to be submitted

"Photo-Assisted Decomposition of Dimethyl Methylphosphonate (DMMP) over Amorphous Manganese Oxide (AMO) Catalysts", Scott R. Segal, Steven L. Suib, Xia Tang and Sunita Satyapal, Chem. Mater., 11, 1687-1695 (1999)

"Photocatalyic Decomposition of DMMP on Titania", Timothy N. Obee and Sunita Satyapal, Journal of Photochemistry and Photobiology A: Chemistry, 1189, 45-51, (1998)

(2) SCIENTIFIC PERSONNEL supported by this project:

Sunita Satyapal (PI, UTRC)
Timothy N. Obee (UTRC)
Xia Tang (UTRC)
Robert Hall (UTRC)
Bruce Laube (UTRC)
Professor Steven Suib (Subcontract to University of Connecticut)
Scott Segal (graduate student)
Lixin Cao (graduate student)

HONORS/AWARDS/DEGREES received during this reporting period:

Lisa Washmon (Masters; Industrial Practicum successfully defended at UT, Dallas)

(3) Report of INVENTIONS (By TITLE ONLY)

Patent disclosures filed:

Synthesis and Application of Carbon-based and Supported Metal-Oxide Catalysts for the Photocatalytic and Thermal Decomposition of DMMP

Novel Applications of Amorphous and Crystalline Manganese Oxide, Vanadium/Vanadium Oxide, Carbon, and P2O5 Catalysts: Photocatalytic and Thermal Destruction of Refrigerants, Chemical Warfare Agents, Organophosphorus Compounds and VOCs

(4) SCIENTIFIC PROGRESS AND ACCOMPLISHMENTS:

Abstract

This report provides a detailed description of results obtained during the third and final year of ARO contract DAAH04-96-C-0067, as well as a summary of results obtained during the entire contract period (see Appendices). During the final year of this program, breakthrough results were obtained on a novel catalyst for the decomposition of DMMP. Previous results during the first two years of the contract had shown catalytic activity from a few minutes to a few hours, *whereas the current catalyst has undergone* ***over 100 hours*** *of continuous operation with no catalytic deactivation.* Two patent applications have been filed (under provisional patent status) based on the novel work conducted under the present contract. In addition to the thermal catalytic work described above, we constructed a photocatlytic reactor prototype for the decomposition of DMMP on titania and conducted detailed reactor modeling to determine reactor size for optimal destruction of DMMP. Three manuscripts for journal publcations were written and are in the process of being submitted. Two additional articles submitted previously were published in 1998 and 1999 respectively and are attached in the Appendix. In addition, students presented portions of this work at the National ACS meeting in California. Results were also presented during a poster session at the International Workshop on Decontamination in a Chemical or Biological Warfare Envirnonment in Durham, England.

Thermocatalytic Oxidation of DMMP

The thermocatalytic oxidation of dimethyl methylphosphonate (DMMP) was carried out on nickel, iron, copper and vanadium oxides supported on various substrates including alumina, silica, and titania. The vanadium catalyst was found to exhibit exceptional catalytic activity, far superior to conventionally well-known platinum catalysts. Varying the vanadium loading from 1 to 15% by weight indicated that 10% vanadium on Al_2O_3 was an optimum concentration. In conjunction with XRD patterns, monolayer dispersion of V_2O_5 on Al_2O_3 was considered to be beneficial to the longevity of these catalysts. Of the various supports studied, including Al_2O_3, SiO_2, and TiO_2, SiO_2 was found to be the optimum support due to its high surface area and its ability to resist poisoning by P_2O_5. On 10% V/SiO_2 catalysts, 100% (to our limit of detection of 0.1%) conversion of DMMP was reached for more than 100 hours at 723 K. IR, XRD, IC, and

XPS results illustrated that the used catalysts contained phosphorus species. The presence of methylphosphonic acid on the catalyst surface and downstream of the packed bed reactor demonstrated the difficulty of P—CH_3 cleavage. The deposition of coke in the catalyst bed and along the reactor wall resulted from the dehydration of methanol and DMMP on P_2O_5. Accumulation of phosphorus species and coke on catalysts gave rise to tremendous loss of surface area. However, P_2O_5 itself was observed to catalyze the decomposition of DMMP. A mechanism for this reaction was proposed to explain these experimental observations. Activated carbon was also found to be effective in the destruction of DMMP above 623 K and a two-stage mechanism involving the formation of P_2O_5 is postulated to explain the high activity.

Summary of Experimental Apparatus and Conditions

Ultra high purity air was used as a carrier gas at a flow rate of 50 mL/min, and flowed through a bubbler filled with DMMP in order to create a vapor stream of DMMP. The concentration of DMMP at 298 K was 1300 ppm (1 Torr). A mass of 0.100 g of catalyst (28-48 mesh) was used for each test. The desired temperatures were controlled by a tubular furnace equipped with a temperature controller. Two GCs were used for on-line analysis. One GC equipped with an FID and RTX-5 column (RESTEK Corp.) was used for analyzing dimethyl ether, methanol, DMMP, and other organic compounds. The other GC equipped with a TCD and Carbowax column (Supelco) was for detecting CO and CO_2 which were decomposition products.

Catalyst Preparation

An impregnation method was employed to synthesize the catalysts. Precursors for the preparation of catalysts were $Ni(NO_3)_2 \cdot 6H_2O$, $Fe(NO_3)_2 \cdot 9H_2O$, $Cu(NO_3)_2 \cdot 2.5H_2O$, NH_4VO_3 and $Pt(acac)_2$. The supports γ-Al_2O_3, and amorphous SiO_2 and P-25 TiO_2 were obtained from Davidson and Degussa respectively. Salts were dissolved in distilled deionized water with the exception of $Pt(acac)_2$, which was dissolved in ethanol. Supports were then added to the solutions and stirred at room temperature for 12 hours. Solutions were evaporated and dried at 393 K. Chunks of samples were ground and then calcined at 723 K for 6 h. Powdered samples were pelletized and sieved into 28-48 mesh granules for catalytic tests.

Characterization Methods

X-ray powder diffraction (XRD) experiments were carried out on a Scintag Model PDS 2000 diffractometer. Samples were loaded onto glass slides, and Cu Kα radiation was used at 45 kV and 40 mA. The sample scans were collected between 5° and 80° 2θ. Diffuse reflectance Fourier transform infrared (FTIR) spectroscopy experiments were performed on a Nicolet 750 spectrometer with a Mercury-Cadmium-Telluride (MCT) detector and KBr beam splitter. Spectra were collected with a resolution of 4 cm^{-1} using 100 scan averages. Surface area measurements were obtained using the BET method with a Micromeritics ASAP 2010 apparatus. The samples were preheated at 423 K under

vacuum before the measurement. Aqueous extraction for ion chromatography analysis was performed by extracting the used catalyst in warm H_2O for at least two hours. The solutions were then treated with ultrasound for 10 min and filtered through 0.22 μm filters. The ion chromatography system contained a Dionex DX 500 ion chromatography pump, a Dionex AS4A-SC anion exchange column and a CD 20 conductivity detector. The eluent contains 1.8 mM Na_2CO_3 and 1.7mM $NaHCO_3$, at an approximate pH of 10. XPS data were obtained with a Physical Electronics ESCA System, Model 5400, equipped with a Mg anode, a hemispherical analyzer, a position sensitive detector and an Omni-fockus lens (nominal area diameters = 1.1 mm and 0.6 mm). All spectra were corrected for sample charging by referring the C1s photoelectron line for adventitious carbon to 284.8 eV.

Results for Thermocatalytic Decomposition of DMMP

Control experiments with an empty reactor over the temperature range 573 K to 723 K showed that the extent of DMMP oxidation at 723 K varied less than 2%. Therefore, it is reasonable to assume that no reaction takes place at temperatures lower than 723 K without a catalyst. Fig.1 shows the time duration of DMMP conversion at 673 K over different metal oxides supported on γ-Al_2O_3. The loading contents of Ni, Fe, Cu, and V were 10% by weight. In this study, 1 wt % Pt/Al_2O_3 catalyst was used for comparison because it has been widely used for the decomposition of DMMP. The "protection time" or "protection period", defined as the period over which 100% conversion of DMMP is maintained, is an important parameter for the evaluation of a catalyst. The sequence of protection times obtained on these catalysts are 10% V/Al_2O_3 (12.5 h) > 1% Pt/Al_2O_3 (8.5 h) > 10% Cu/Al_2O_3 (7.5 h) > Al_2O_3 (4.0 h) > 10% Fe/Al_2O_3 (3.5 h) > 10% Ni/Al_2O_3 (1.5 h).

The vanadium catalyst exhibited higher catalytic activity than any other catalysts examined here. After passing the protection period, nickel, iron and bare Al_2O_3 catalysts lost activity abruptly. The conversion of DMMP actually increased after 17 h on the 10% V/Al_2O_3 catalyst and is explained as follows. In our experiments, we observed the formation of significant amounts of coke initially on the catalyst bed and later along the reactor walls. We eventually discovered that the coke was generated via dehydration of methanol and DMMP on P_2O_5, a product from the decomposition of DMMP. Thus, the accumulated P_2O_5 along the reactor wall was able to catalyze the decomposition of DMMP to form coke. After passing through the protection period, P_2O_5 started to function as a catalyst, which led to the increase in conversion of DMMP (about 98%). Another notworthy point is that with the 10% V/Al_2O_3 catalyst, a "white fog" was observed in the reactor exit gas stream. The white fog was trapped with water for ion chromatography analysis and was found to primarily contain dissolved MPA.

Fig.1 shows that platinized Al_2O_3, as a reference catalyst, is more active than copper, nickel, and iron catalysts, but not as active as vanadium catalysts. The protection time of 4 hours obtained on bare γ-Al_2O_3 could be due to the stoichiometric reaction between Al_2O_3 and DMMP. The protection times of nickel and iron catalysts were shorter than those on bare Al_2O_3. The explanation for this observation is that bulk Al_2O_3

was covered by the phosphorus-poisoned iron, or nickel compounds (such as $FePO_4$, or $Ni_3(PO_4)_2$), which hindered further exposure of Al_2O_3 to DMMP.

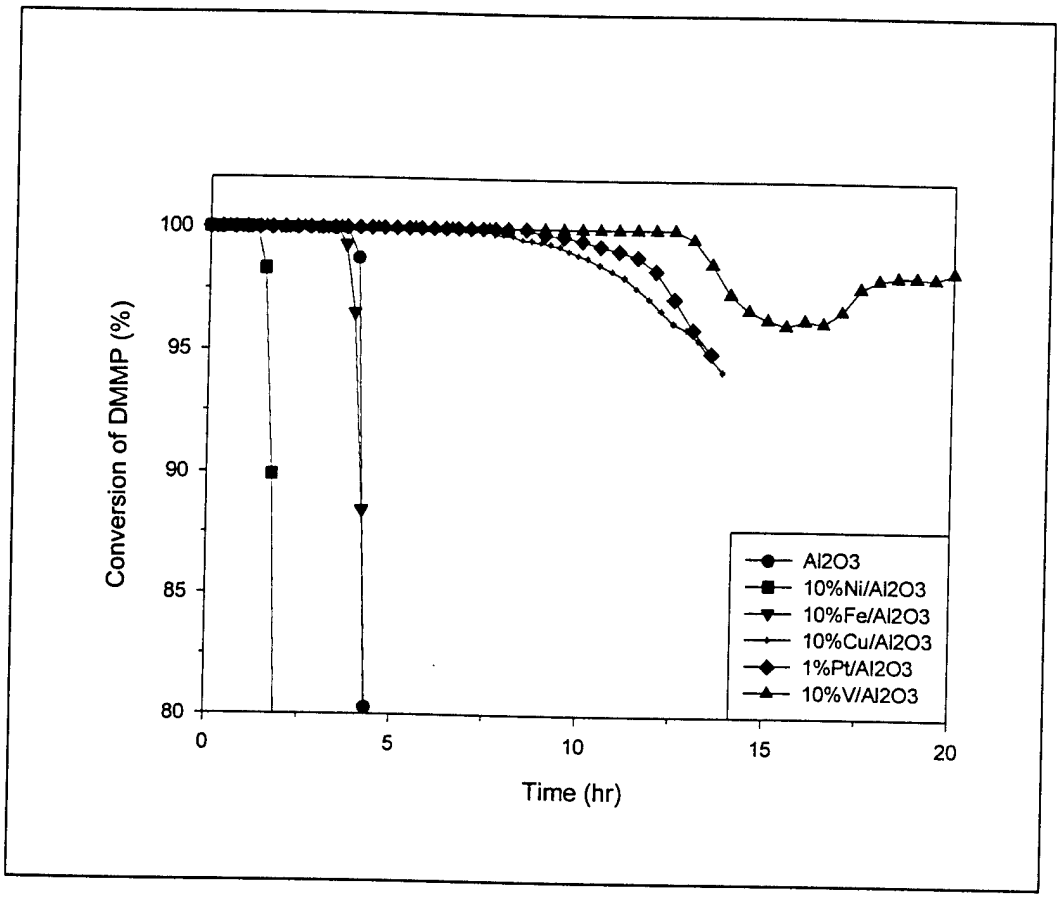

Fig. 1. Time course of DMMP conversion over different catalysts at 673 K. Inlet DMMP concentration, 1300 ppm; total flow rate: 50 mL/min.

Fig. 2 shows the variation of methanol concentrations in the flowing stream with reaction time. In general, we find that detection of methanol intermediate directly correlates with a decrease in DMMP conversion. Therefore, the trend shown in Fig. 2 is opposite to that in Fig. 1. The difference among those catalysts is that a small amount of methanol was observed on the vanadium catalyst, even during the protection period. After 15 h, the irregular change in methanol concentration on 10% V/Al_2O_3 is ascribed to catalytic effects of the formed P_2O_5. On Al_2O_3, trace dimethyl ether (DME) was detected in the beginning of the reaction. The DME vanished soon after with an increase in methanol.

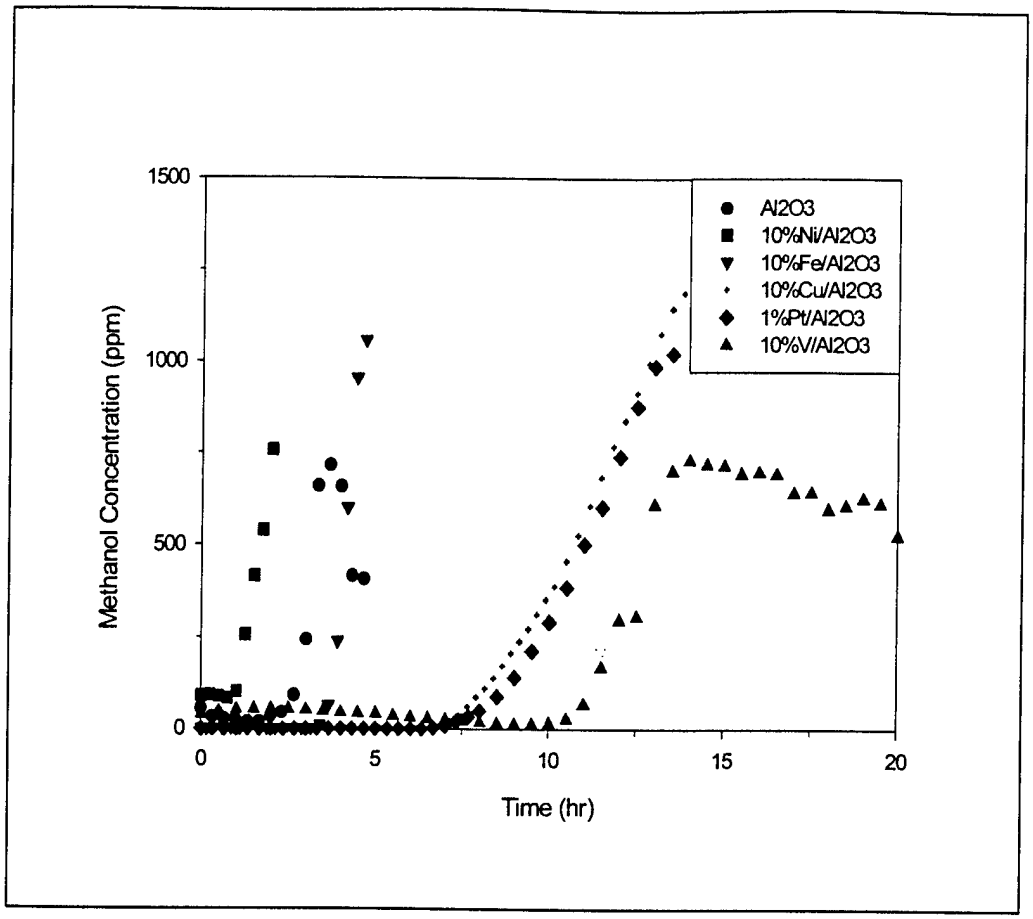

Fig. 2. Methanol concentration as a function of time on stream. Reaction temperature, 673 K; inlet DMMP concentration, 1300 ppm; total flow rate, 50 mL/min.

The CO_2 concentrations against reaction time were also measured. The 1% Pt/Al_2O_3 catalyst exhibits large amounts of CO_2 production. During the protection period, an approximately 100% carbon balance was obtained only on the 1% Pt/Al_2O_3 catalyst, as compared to all other catalysts tested. Note that the 10% V/Al_2O_3 catalyst which showed the best conversion of DMMP generated very low CO_2. The carbon balance on this catalyst was much less than 100%. The majority of carbon in DMMP was converted to coke deposited on the catalyst and downstream (along the reactor walls).

Since the vanadium catalyst was found to be an excellent candidate for oxidation of DMMP, the effects of vanadium concentration on catalytic activity were investigated in order to find a catalyst with high activity and low metal loading (see Fig. 3). The protection times as a function of V concentration were found to be 10% (12.5 h) > 5% (11.5 h) > 1% (9.5 h) > 15% (8 h). Compared to the 5% V/Al_2O_3 catalyst, the protection time of 10% V/Al_2O_3 increased by only one hour although the content of vanadium was doubled. Furthermore, a short protection time was obtained on 15% V/Al_2O_3. This observation reveals that high loadings do not benefit the activity of catalysts. An interpretation of this trend is that high loading decreases the surface areas (shown in Table 1), in particular for the sample with loading content up to 15%. Pure V_2O_5 with a

surface area of 1.6 m^2/g did not show activity since the protection time was less than half an hour. Unlike the 10% V/Al_2O_3 sample, no rebound in conversion of DMMP occurred on the 15%, 5% and 1% vanadium catalysts. During the protection period, the product distribution of methanol on these four samples was very similar, approximately 50 ppm. The concentrations of CO_2 were 360 ppm, 250 ppm, 130 ppm and 150 ppm on the 1%, 5% 10%, 15% V/Al_2O_3 catalysts, respectively. The protection time using the 1% V/Al_2O_3 catalyst (9.5 h) was found to be one hour longer than that for the 1% Pt/Al_2O_3 catalyst (8.5 h). In other words, the high activity and low loading levels for the vanadium catalyst imply that these vanadium catalysts may be of practical interest for replacing platinum catalysts for the catalytic oxidation of DMMP.

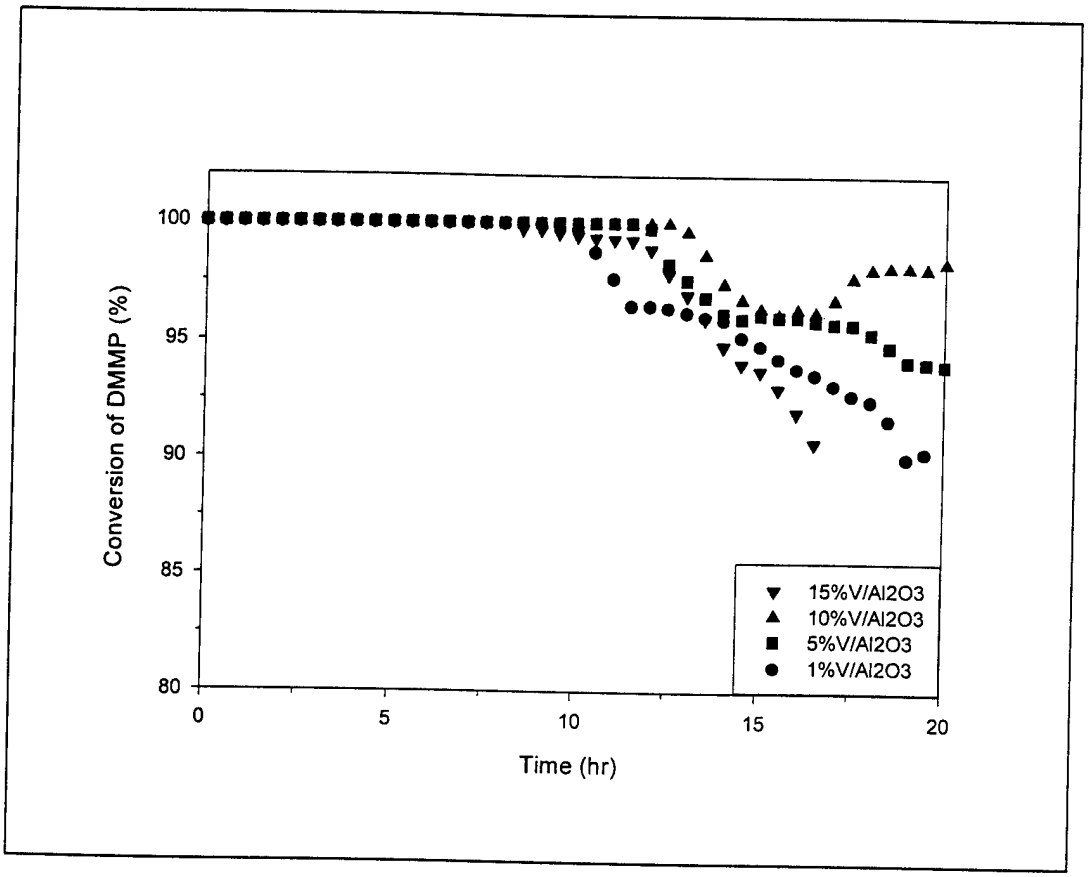

Fig. 3. Effects of vanadium loading on protection time. Reaction temperature, 673 K; inlet DMMP concentration, 1300 ppm; total flow rate, 50 mL/min.

Table 1. BET surface areas of supports, fresh, and used catalysts.

Catalysts	Surface Areas of Fresh Catalysts (m^2/g)	Surface of Areas of Used Catalysts (m^2/g)	Reaction Time (hour)
SiO_2	262.2		
TiO_2	50.2		
V_2O_5	1.6		
Al_2O_3	289.2	3.8	5
10% Cu/Al_2O_3	229.6	59.0	14
10% Fe/Al_2O_3	223.8	136.8	5
10% Ni/Al_2O_3	227.7	159.2	2
1% Pt/Al_2O_3	284.8	13.2	14
1% V/Al_2O_3	272.6	7.9	20
5% V/Al_2O_3	255.9	11.2	50
10% V/Al_2O_3	248.8	4.3	100
15% V/Al_2O_3	203.8	16.5	20
10% V/TiO_2	29.9	24.4	9
10% V/SiO_2	190.4	10.6	100

Activity as a Function of Catalyst Support

The disadvantage of using γ-Al_2O_3 as a support is that basic γ-Al_2O_3 is able to react with acidic P_2O_5 to form $AlPO_4$, which can give rise to a drastic loss of surface area. For comparison, the relatively acidic supports, such as SiO_2, and TiO_2, were chosen in this study. Fig. 4 shows the conversion of DMMP on vanadium (10 wt %) catalysts supported on Al_2O_3, SiO_2 and TiO_2. XRD results demonstrated that SiO_2 was amorphous and that commercially available P-25 TiO_2 is a mixture of anatase and rutile with a ratio of 75:25, as confirmed in the literature. The catalytic activity was markedly enhanced

using SiO_2 for which a protection time of 25 h was obtained. This catalyst was actually run for 100h. After passing through the protection time, the 10% V/SiO_2 catalyst deactivated slightly and the conversion of DMMP fluctuated within 99-100%. However, the 10% V/TiO_2 catalyst deactivated very quickly. The low surface area of this catalyst (29.9 m^2/g) may be the explanation of poor activity. Lee et al. [1] reported that Pt/TiO_2 was not as effective as Pt/Al_2O_3. The methanol concentrations were maintained at an average level of 50 ppm, 250 ppm and 750 ppm on Al_2O_3, SiO_2 and TiO_2 catalysts, respectively. The CO_2 concentrations were 130 ppm and 250 ppm on Al_2O_3 and SiO_2 catalysts, respectively. A trace amount of CO_2 was obtained on the TiO_2 catalyst. Pure SiO_2 and TiO_2 supports did not exhibit catalytic activity. Thus, is summary, 10% vanadium supported on SiO_2 was the best catalyst we have found for the decomposition of DMMP.

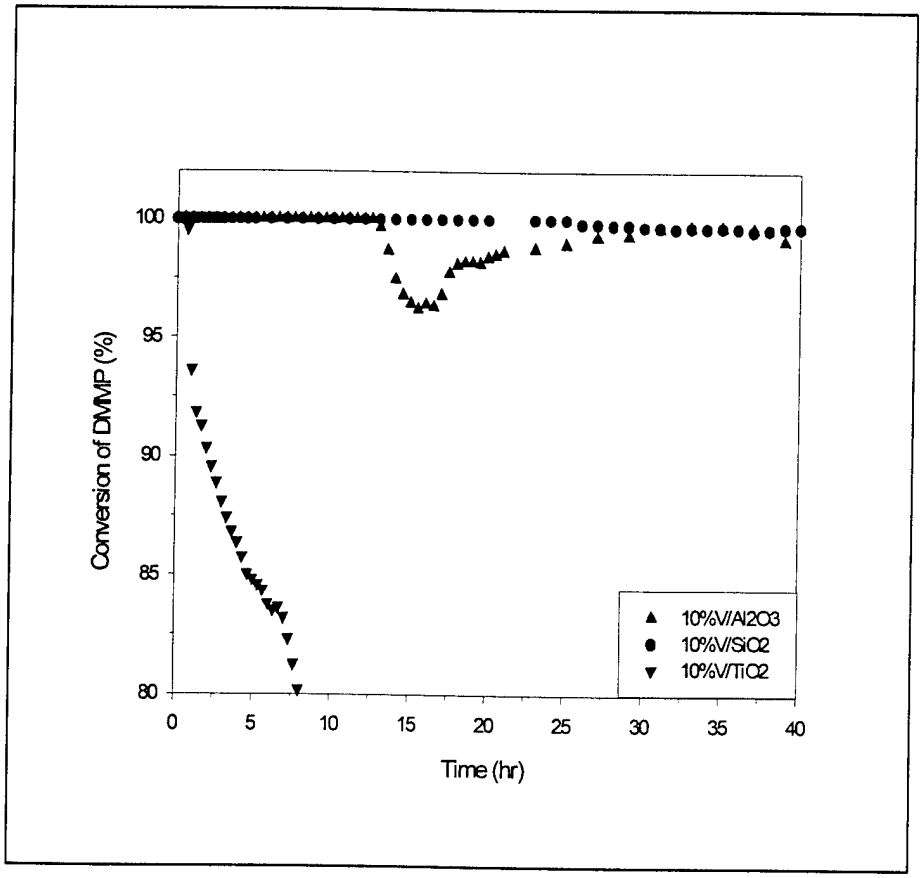

Fig. 4. Effects of supports on protection time. Reaction temperature, 673 K; inlet DMMP concentration, 1300 ppm; total flow rate, 50 mL/min.

Temperature dependence

The oxidation of DMMP is a particularly temperature sensitive reaction because the decomposition product P_2O_5 has a high sublimation point (623 K). Low temperatures will therefore result in the accumulation of phosphorus species on catalyst surfaces. In order to investigate the effects of temperature on catalytic activity, temperature dependent experiments were conducted on the 10% V/SiO_2 catalyst and these results are presented in Fig. 5. The protection times at 623 K, 673 K and 723 K were 5 h, 25 h and >100 h respectively. At a temperature as low as 623 K, accumulated phosphorus species on catalyst surfaces led to a drastic loss of active sites and surface area. This could be the main reason for the deactivation of the catalyst at such low temperatures. In contrast, the catalyst survived more than 100 h at 723 K. The concentration of CO_2 at 723 K was approximately 750 ppm. Small amounts of effluent methanol were detected (about 25 ppm). Coke was formed on the catalyst and along the reactor wall. In comparison, Graven et al. [2] examined the effect of temperature on deactivation over 0.5% Pt/Al_2O_3 catalysts and found that deactivation was still observed at 717 K under their reaction conditions.

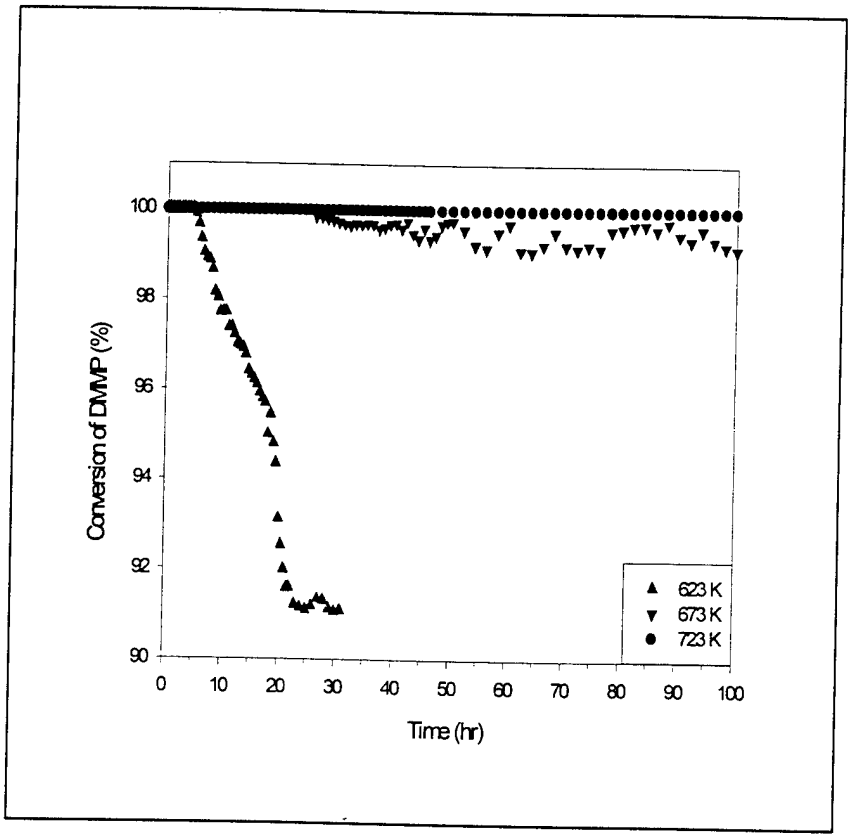

Fig. 5. Temperature dependence of oxidative decomposition on 10% V/SiO_2. Inlet DMMP concentration, 1300 ppm; total flow rate, 50 mL/min.

BET surface areas

The BET surface areas of fresh and used catalysts are listed in Table 1. All the used catalysts were run at 673 K for different times until they deactivated. The data for the 10% V/SiO_2 catalyst, which was tested at 723 K for 100 h, was not available because the catalyst was firmly stuck to the reactor wall and could not be removed. The bare Al_2O_3 lost its surface area very quickly (from 289 to 3.8 m^2/g) in 5 h because of the stoichiometric reaction between Al_2O_3 and DMMP. The high surface areas of the used 10% Cu/Al_2O_3 and 10% Fe/Al_2O_3 catalysts are due to their short reaction times related to their protection times (shown in Fig. 1). Investigation of the relationship between vanadium loading content and surface area indicates that increasing loading contents (from 1% to 15%) gives rise to a decrease in surface area. After a 100 h run, both 10% V/Al_2O_3 and 10% V/SiO_2 samples lost almost all their surface area. The accumulation of phosphorus-bearing compounds and coke may be the explanation of this observation. In general, a support with low surface area, such as TiO_2, is not suitable for this reaction.

Fourier Transform Infrared Experiments

Investigation of the surface species on the catalysts before and after reaction was performed using FT-IR and the results are presented in Fig. 6. Spectrum A indicates that the fresh γ-Al_2O_3 contains large amounts of water. The broad band spanning over the range of 3700-2500 cm^{-1} is assigned to —OH stretches. Correspondingly, an —OH bend appears at 1643 cm^{-1}. An Al—O vibration is indicated by a broad band at 1036 cm^{-1}. The deactivated Al_2O_3 shown in spectra B contains a P—CH_3 moiety (ν_a: 3002 cm^{-1}, ν_s: 2936 cm^{-1}, δ_a: 1418 cm^{-1}, δ_s: 1321 cm^{-1}), which has been explicitly illustrated by many authors [see for example, ref. 3]. The band at 1230 cm^{-1} indicates the presence of P=O [4]. Corbridge et al. [5] pointed out that (P)—O—H stretch falls into two regions: 3000-2525 cm^{-1} and 2400-2000 cm^{-1}. Three peaks appear at 2319, 2223, and 2106 cm^{-1} and are assigned to a (P)—O—H stretch. Two bands with wave numbers as high as 3832 and 3903 cm^{-1} are difficult to assign and may be combination bands. Comparison of spectra D (fresh 10% V/Al_2O_3 catalyst) and spectra C (used catalyst) indicates the presence of P—CH_3, with two bands in the region of 3000-2900 cm^{-1} on the surface of the deactivated catalyst. In spectrum D, a striking band at 2345 cm^{-1} is due to the (P)—O—H stretch. Correspondingly, a (P)—O—H deformation appears at 1393 cm^{-1}. A weak adsorption at 1224 cm^{-1} is due to a P=O stretch. Another significant difference between spectra C and D is the disappearance of an Al—O vibration near 1036 cm^{-1}. Note also, that at the high reaction temperatures (300-450 deg C), water will be desorbed from the surface. This observation demonstrates that the poisoning of γ-Al_2O_3 by phosphorus species resulted in a structural change of Al_2O_3. Because of destruction of the hydrophilic surface of γ-Al_2O_3, the deactivated sample no longer contains physisorbed water, which is illustrated by the disappearance of the —OH vibration (stretch in the range 3700-2500 cm^{-1} and bend at 1643 cm^{-1}). In contrast, the SiO_2 surface is resistant to poisoning of phosphorus containing compounds.

No obvious (P)—O—H band was observed in spite of the presence of trace P—CH_3 moieties. However, the surface still lost water and free (Si)—O—H groups (3747 cm^{-1}).

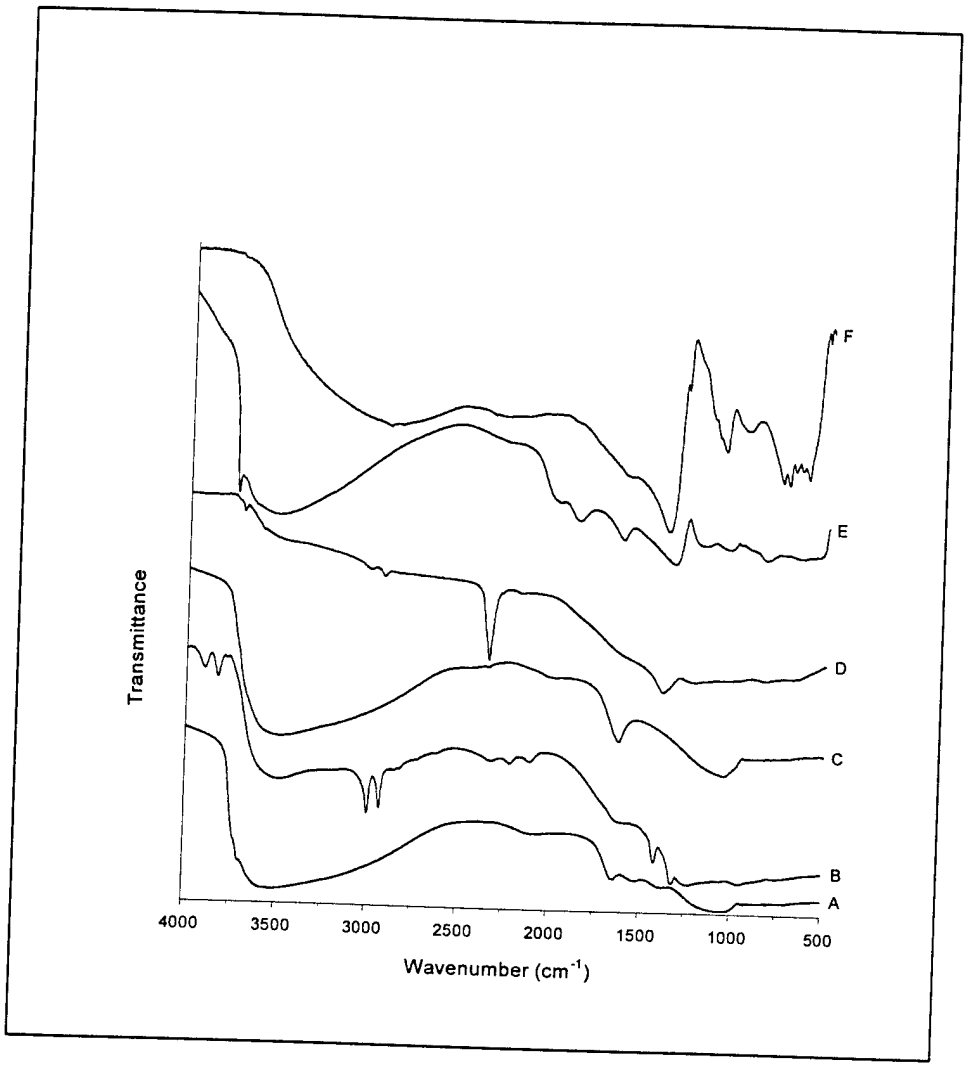

Fig. 6. Diffuse reflectance FTIR spectra for fresh and used catalysts. (A) γ-Al_2O_3; (B) used γ-Al_2O_3; (C) 10% V/Al_2O_3; (D) used 10% V/Al_2O_3; (E) 10% V/SiO_2; (F) used 10% V/SiO_2.

X-ray Diffraction Results

XRD patterns for different samples are shown in Fig. 7. The characteristic indices of crystalline V_2O_5 were observed over 10% and 15% V/Al_2O_3 catalysts (patterns C and D). In particular, bulk V_2O_5 was obviously present on the 15% V/Al_2O_3 catalyst. However, no such characteristic indices were observed if the loading content of V_2O_5 was lower than 5%.

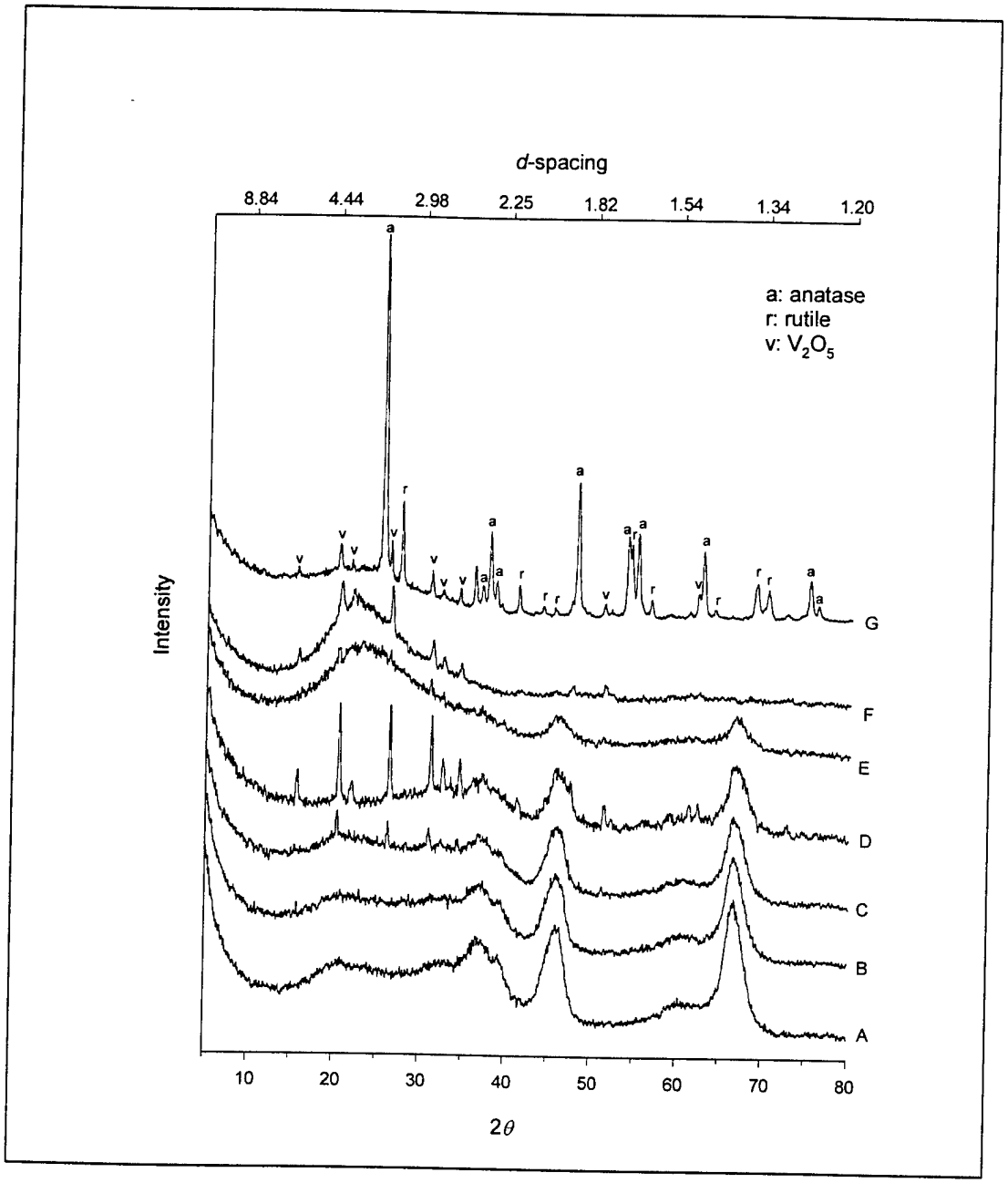

Fig. 7. X-ray patterns for different vanadium catalysts. (A) 1% V/Al_2O_3; (B) 5% V/Al_2O_3; (C) 10% V/Al_2O_3; (D) 15% V/Al_2O_3; (E) used 10% V/Al_2O_3; (F) 10% V/SiO_2; (G) 10% V/TiO_2.

It is reasonable to assume that V_2O_5 is dispersed on Al_2O_3 as a monolayer. On amorphous SiO_2 with a surface area of 262.2 m^2/g, a small amount of bulk V_2O_5 was observed. Two types of TiO_2 crystallinity, anatase and rutile, as well as V_2O_5 were presented on the 10% V/TiO_2 catalyst. Comparison of the used and fresh catalysts indicates that a phase transformation occurred on the used 10% V/Al_2O_3 catalyst (Pattern E). The broad peak with a d-spacing of 4.23 is probably due to the formation of noncrystalline $AlPO_4$. The results are in good agreement with a report by Baier et al. [6]. In combination with BET results, we believe that the formation of $AlPO_4$ is the reason for the decrease in surface area of the used Al_2O_3 systems.

Ion Chromatography Results

Ion chromatography was used to detect PO_4^{3-}, methyl phosphonate acid (MPA), and methyl methylphosphonate (MMP) on different samples. Samples were extracted with water prior to analysis. Thus, only water-soluble species could be detected using this method. However, DMMP was undetectable because of its nonconductivity in water. The used 10% V/SiO_2 catalyst contained more PO_4^{3-} than the 10% V/Al_2O_3 catalyst despite the same reaction time (100 h) and reaction temperature (673 K). This is due to the presence of $AlPO_4$, which is insoluble in water and thus can not be measured. The coke scraped from the reactor wall contained a large amount of PO_4^{3-}, probably from the hydrolysis of P_2O_5, as well as trace MMP. The "white fog" from the outlet of the reactor was collected for 50 h using distilled water. PO_4^{3-}, MPA, and trace MMP were detected. Compared with PO_4^{3-}, MPA was present in large amounts, providing additional evidence of the difficulty in cleaving P—CH_3 bonds.

XPS spectra

XPS spectra for the used 10% V/SiO_2 materials are shown in Fig. 8. The binding energies for specific elements are labeled on the corresponding peaks. In comparison to the fresh catalyst, the used catalyst obviously contains two new elements: phosphorus and carbon, which are illustrated by the binding energies of 134.2 eV for P 2p and 284.8 eV for C 1s. The binding energy for phosphorus indicates that phosphorus is mostly in the form of PO_4^{3-}. This is in good agreement with our IC results. The binding energy for carbon is consistent with that for graphitic carbon. The surface concentrations (atom %) of the used catalyst are 65.6% (O), 1.0% (V), 5.5% (P), 18.2% (P), and 9.7% (Si).

Mechanism

The detailed characterization experiments described above were valuable for determining the mechanism for decomposition, which is in turn of value to design better catalysts. Our results show that high surface area (262.2 m^2/g) and inertness to P_2O_5 make SiO_2 an excellent support for V_2O_5 dispersion. Thus, the 10% V/SiO_2 catalyst exhibits exceptional activity for the catalytic decomposition of DMMP. Although γ-Al_2O_3 has a high surface area, 289.2 m^2/g, it is not resistant to the poisoning of acidic P_2O_5.

During the course of the reaction, the formation of $AlPO_4$ led to the collapse of crystalline γ-Al_2O_3 [6]. On the other hand, although TiO_2 is inert to P_2O_5 poisoning, the low surface area (50.2 m^2/g) inherently limits the catalytic activity. In practical use, neither of these two supports is suitable for catalyst preparation.

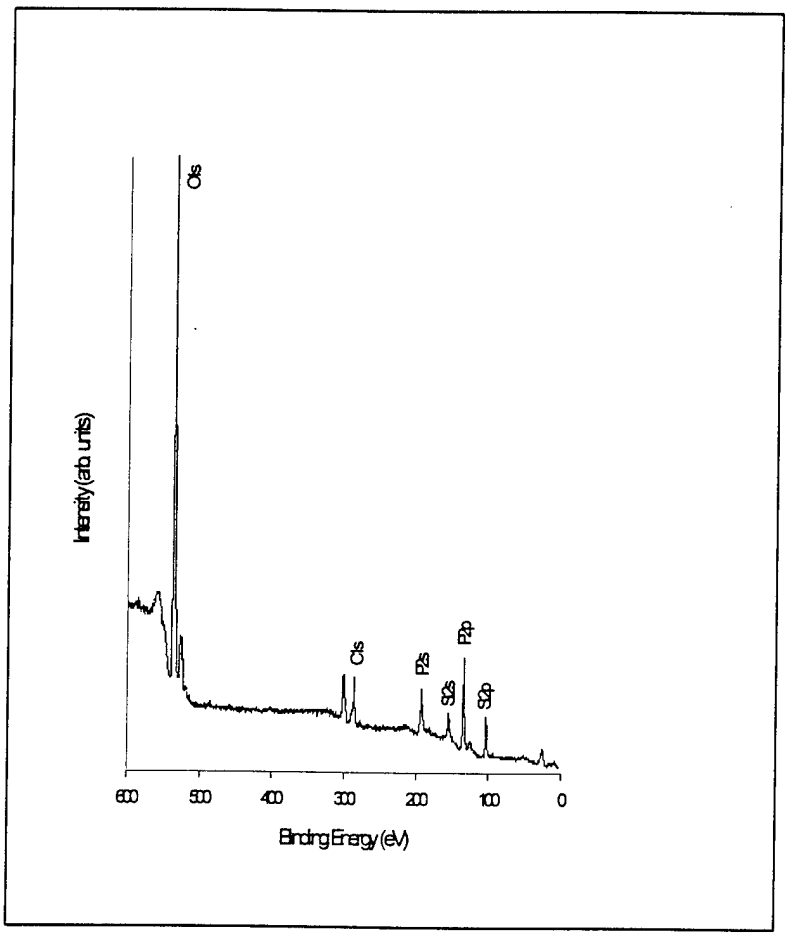

Fig. 8. XPS spectrum of the used 10% V/SiO_2 catalyst (100 h).

Our experiments indicate that the P—CH_3 bond is hard to cleave even though the majority of DMMP is decomposed into phosphorus oxide or phosphate. Thus, the suggested scheme for the process of DMMP decomposition is: DMMP $\rightarrow$ MMP $\rightarrow$ MPA $\rightarrow$ PA (phosphoric acid). At high temperature, phosphoric acid may exist as P_2O_5 as a result of dehydration.

The following scheme (1-4) is suggested to explain the reaction processes:
In the beginning of the reaction, DMMP is catalytically converted to methanol, CO_2, and P_2O_5 in the presence of oxygen (Step 1). Subsequently, P_2O_5 can react with metal oxides to form phosphates (Step 2). If more P_2O_5 is accumulated on the catalyst or condensed along the reactor wall, it is able to catalyze the decomposition of DMMP to form new P_2O_5 and other products (Step 3) since P_2O_5 is a strong desiccant and is able to extract water even from organic compounds. The assumptions have been confirmed by the following experiments:

Experiment 1: More than 90% conversion of DMMP was obtained at 673 K when an air stream with DMMP vapor passed through the pure P_2O_5 bed in the absence of any aforementioned catalysts. P_2O_5 sublimed slowly and then condensed on the downstream reactor wall. Coke was observed as the major product and formed in the same region containing P_2O_5. Methanol and CO_2 were present in small amounts.

Experiment 2: If the carrier gas (air) was replace with helium, high conversion of DMMP (~90%) and coke was still obtained on P_2O_5. Instead of CO_2, dimethyl ether and methanol were observed.

$$\text{DMMP} + O_2 \xrightarrow{\text{Catalyst}} \text{Methanol} + CO_2 + P_2O_5 \qquad (1)$$

$$P_2O_5 + \text{Metal Oxide} \longrightarrow \text{Phosphate} \qquad (2)$$

$$\text{DMMP} + O_2 \xrightarrow{P_2O_5} \text{Methanol} + CO_2 + \text{Coke} + P_2O_5 \qquad (3)$$

$$\text{Methanol} \xrightarrow{P_2O_5} \text{Coke} + CO_2 \qquad (4)$$

Experiment 3: Coke was formed at 673 K on P_2O_5 if DMMP was replaced with methanol vapor.

Experiments 1 and 3 verify the appropriateness of Steps 3 and 4, respectively. Experiment 2 demonstrates that P_2O_5 can remove molecular water from DMMP without the assistance of oxygen. However, the detection of CO_2 and methanol, instead of dimethyl ether, in the oxidation of DMMP demonstrate that the key reaction proceeds via Step 3 after P_2O_5 starts to function as a catalyst. Over vanadium catalysts, (e.g. 10% V/SiO_2) the reaction proceeds as in Step 1. P_2O_5 accumulates in the catalyst bed at the start of DMMP decomposition since V_2O_5 and SiO_2 are resistant to P_2O_5. After the vanadium catalyst passes the protection period, Step 3 actually dominates the reaction because the accumulated P_2O_5 begins to catalyze the oxidation of DMMP. The conversion of DMMP at this stage is not absolutely 100% (99 ~ 100%, Fig. 5). The prerequisite for Step 3 is adequate accumulation of P_2O_5. Therefore, the long protection time achieved with 10% V/Al_2O_3 and 10% V/SiO2 catalysts is due to the combination of the original

vanadium catalysts and subsequent P_2O_5. However, on other metal oxides (NiO, Fe_2O_3, and CuO) as well as Al_2O_3 supported catalysts, the combining effects of both catalysts and P_2O_5 is disrupted because of consumption of P_2O_5 in Step 2. Insufficient P_2O_5 is generated during the protection period for subsequent DMMP decomposition. This conclusion can be used to interpret the data for the 10% V/Al_2O_3 catalyst in Fig. 1. If a catalyst can not survive for a sufficient time to provide enough P_2O_5, the conversion of DMMP will abruptly decrease after the protection time. The unusual behavior of the 10% V/SiO_2 catalyst is due to the resistance of both the active component (V_2O_5) and the support (SiO_2) against the poisoning of P_2O_5. Therefore, P_2O_5 plays two totally different roles for different catalysts: (1) P_2O_5 can poison catalysts to form phosphates if the active components or supports are able to react with acidic P_2O_5; (2) Instead, P_2O_5 can assist to decompose DMMP if a certain amount of P_2O_5 is accumulated in a reactor. To the best of our knowledge, such data and corresponding explanations have not been previously reported.

Activated Carbon

In addition to the above-described vanadium catalysts, we have found that activated carbon is similarly effective in decomposing DMMP with high (~100%) efficiency. The activated carbon used in this study was obtained from Strem Chemicals, Inc. The granular activated carbon was cracked into 28-48 mesh particles for activity tests. The BET surface area was 897.5 m^2/g, with a pore volume of 0.6033 cm^3/g. After being degassed at 300 °C for 10 hours, the activated carbon lost 18.5% of its weight due to water desorption. After reaction, the activated carbon lost the majority of its micropores as its surface area and total pore volume decreased (897.5 to 241.3 m^2/g). Although the total pore volume decreased, the macropore volume increased.

During the course of the reaction, large amounts of phosphorus species and coke occupied the pores resulting in a sharp decrease in pore volume and surface area. Experimental results showed that the decomposition of DMMP involved two stages. In the first stage, activated carbon behaved as an initiator converting DMMP into CO_2, methanol, and P_2O_5. This reaction required oxygen supplied from air. In the second stage, P_2O_5 accumulated in the reactor was able to catalyze the decomposition of DMMP. The second stage was actually an autocatalytic process.

As the experiment is initiated (see Fig. 9), the activated carbon is relatively stable in flowing air at temperatures below 673 K. A 'burning' process then occurs and releases CO_2 at 723 K. After 5 h of reaction above 673 K, the activated carbon loses its porosity and surface area almost completely. However, the conversion of DMMP remains above 99% for 100 h. The prolonged apparent protection time is contributed to by both the activated carbon catalyst and the P_2O_5 formed in the reaction process. This autocatalytic reaction is temperature dependent since high temperature facilitates cleavage of the P—CH_3 bond.

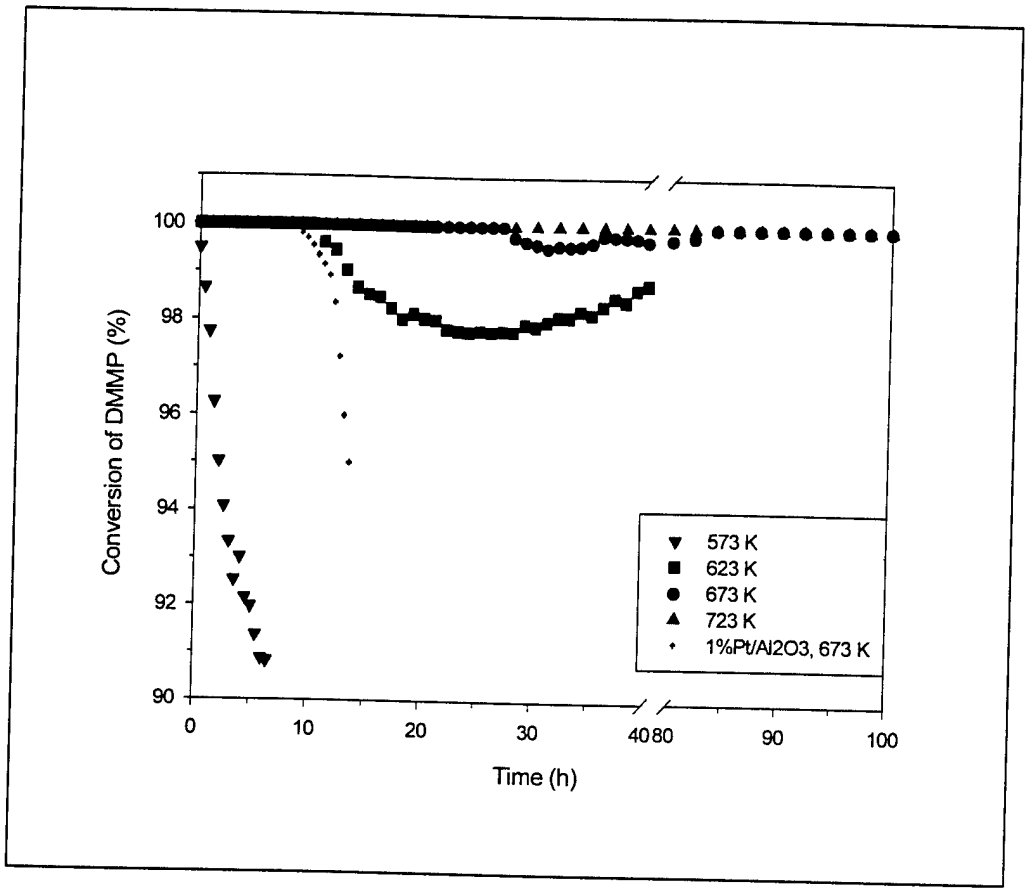

Fig. 9 Conversion Efficiency for DMMP On Activated Carbon.

Photocatalytic Experiments

In addition to the thermally activated catalytic experiments described above, we also investigated the photocatalytic decomposition of DMMP. The catalyst used was titania and the details of the experimental set up are shown in the Appendix.

In order to design a photocatalytic reactor for the destruction of CWAs, the intrinisc or kinetic rates of reaction must be determined. We have done this using the data generated with UTRC's intrinsic rate reactor. The oxidation rate was defined by

$$r = 2.45\,(X_{in} - X_{out})\,Q / A$$

where r (μ-mole/cm^2-hr) is the oxidation rate; and X_{in} (ppm) and X_{out} (ppm) are the inlet and outlet DMMP concentrations, respectively; Q (lpm) is the volumetric flow rate; and A (cm^2) is the area of the titania-coated glass-plate; the numerical coefficient accounts for the units change.

Intrinsic rate determinations were performed at a 4 lpm flow rate. To check for gas-side mass-transfer influence, the flow was doubled to 8 lpm. The subsequent oxidation rate remained unchanged indicating that the oxidation rates obtained at the 4 lpm flow were free of gas-side mass-transfer influences. For the generation of intrinsic rates, the relative fractional change in the DMMP concentration through the reactor was maintained below 0.1 through the selection of an appropriate catalyst (slide) length. This ensured that the reactor was being operated in a differential mode during intrinsic rate determinations.

In all photooxidation experiments the following protocol was used: First, the gas flows, DMMP, and water vapor levels were set. When the inlet/outlet DMMP concentrations reached steady-state and were of equal magnitude, the UV lamp was illuminated.

For the study of possible homogeneous reactions, uncoated glass-slides were placed in the reactor. The lamp type (germicidal or ozone), irradiation intensity, DMMP, and oxygen level were varied. No change in DMMP, carbon dioxide, or carbon monoxide level through the reactor was seen when irradiated with the germicidal lamp. For the ozone lamp, a change in DMMP concentration through the reactor was observed, even in the absence of oxygen, indicating the presence of direct photo-dissociation. The change in DMMP monotonically increased with increasing oxygen level up to the highest oxygen level used.

Catalyst deactivation due to the reaction of DMMP was first observed under black-light irradiation as discussed in our previous paper (see Appendix). In that study, rejuvenation of the catalyst was accomplished by simply washing the catalyst with water. The photooxidation of DMMP under germicidal and ozone lamps irradiation also resulted in deactivation of the catalyst. The oxidation rate from the germicidal and ozone lamps did not differ significantly, and could be the result of the low irradiation level used and concomitant low ozone level. A performance comparison for these two lamps at the maximum available irradiation level is shown in Fig. 10. In spite of a high ozone level with the ozone lamp and an expected concomitant ΔDMMP of 0.8 ppm from the homogeneous reaction pathway, there was no significant difference between the two lamp types.

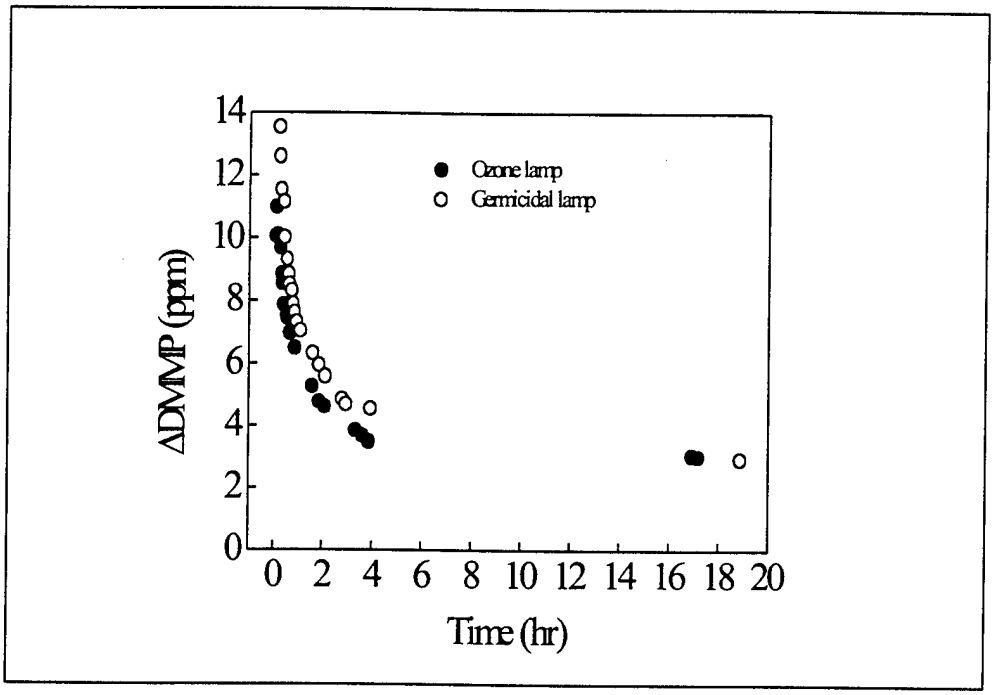

Fig. 10 Effect of lamp type on DMMP disappearance: 38 m W/cm^2 @ 254 nm, 42 ppm DMMP influent, 6500 ppmv humidity.

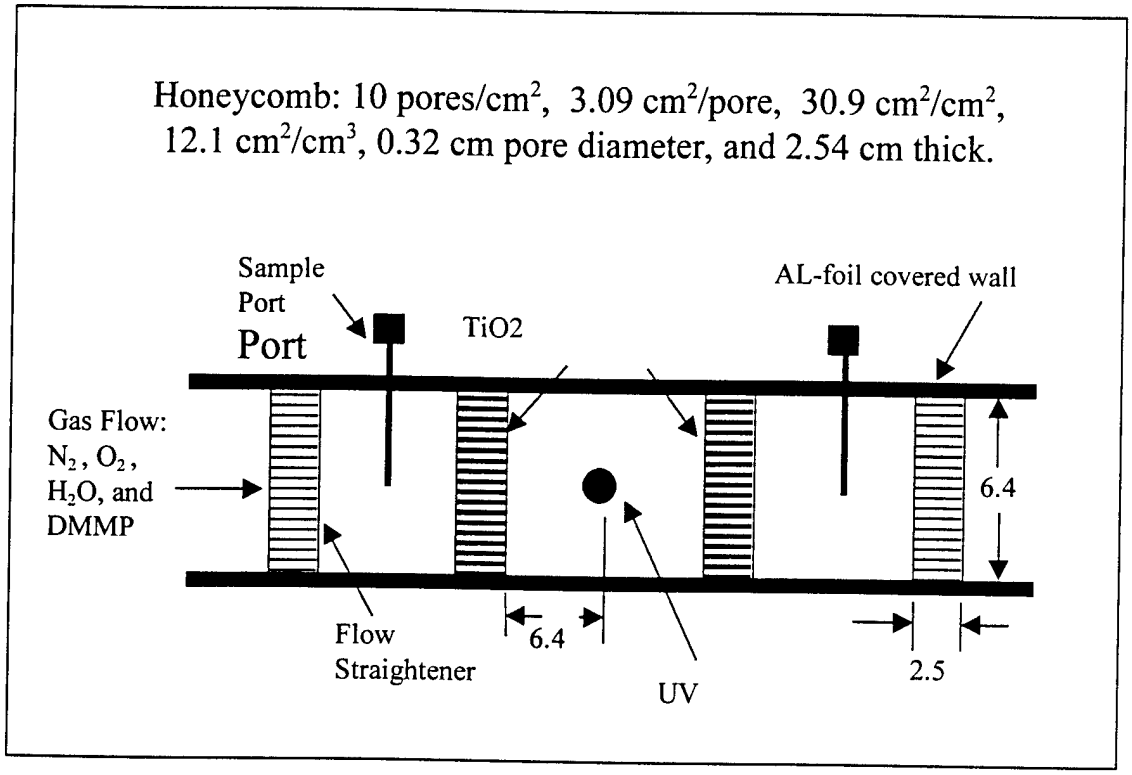

Figure 11 DMMP Demonstration Reactor.

DMMP Demonstration Photocatalytic Reactor

For the study of possible homogeneous reactions, uncoated honeycombs were substituted for the coated honeycombs in the demonstration reactor (Fig. 11). The lamp type (black-light, germicidal or ozone), oxygen level, and flow rate were varied. No change in DMMP, carbon dioxide, or carbon monoxide level through the reactor was measured when irradiated with the black-light or germicidal lamps. For the ozone lamp, a change in DMMP concentration through the reactor was observed and is shown in Table 2. The change in DMMP at zero oxygen indicated the presence of significant direct photo-dissociation. The addition of oxygen (20%) generated ozone and resulted in a further increased in the rate of DMMP disappearance. The high ozone level, compared to those seen in the intrinsic reactor, was a consequence of the lamp sitting in the flow field and subsequently a greater volumetric generation of ozone was produced. The presence of ozone suppressed the formation of carbon dioxide but enhanced the formation of carbon monoxide.

The performance characteristics of the UV lamps are shown in Table 3. The UV intensity is given as that at the entrance plane of the honeycombs, that is, 6.4 cm from the lamp. Although the black-light lamp produce half the intensity of either the germicidal or ozone lamps, the power used by the lamps was nearly the same. The total UV power was computed by treating the lamp as a line source and integrating about a cylinder enclosing the lamp. The result of the integration is an equation (see Table 2) relating the total UV power to the UV flux at any centered distance from the lamp. The total length of each lamp was 38 cm for the black-light lamp, and 28 cm for the germicidal and ozone lamps. The interior of the reactor was exposed to only 6.4 cm of these total lamp lengths.

For the study of photocatalytic reactions, two titania coated honeycombs were placed in the reactor (Figure 11). The lamp type (black-light, germicidal or ozone) and flow rate were varied, while the oxygen level was fixed at 20%. The results are shown in Table 4. Reliable carbon dioxide or carbon monoxide levels could not be determined with the ozone lamp only and are not so reported in Table 4. The greatest DMMP disappearance was recorded with the ozone lamp. For the ozone lamp and 24 lpm flow rate, the 100% DMMP disappearance could be roughly distributed as follows: direct dissociation 27%, direct dissociation plus ozone reactions was 58%, the balance, if attributed to photocatalytic processes alone, would be 42%. For the ozone lamp and 12 lpm flow rate, the 100% DMMP disappearance was brought about without photocatalytic processes; direct dissociation 57%, direct dissociation plus ozone reactions was 100%. With respect to the power consumed by the lamps, the effect of the UV lamp type on DMMP disappearance followed the order: ozone-lamp > germicidal-lamp > black-light-lamp. No attempt was made to determine the quantum efficiency of these lamps.

Table 2 Homogeneous DMMP disappearance for variations in oxygen and flow rate

#	Flow Rate (lpm)	Water Vapor (ppm)	O_2 (%)	Ozone (ppm)	DMMP (ppm)	ΔDMMP (ppm)	ΔCO2 (ppm)	ΔCO (ppm)	Eff. (%)
1.	12.1	5600	20	33.0	2.03	2.03	0.00	1.10	100
2.	12.1	5300	0	0.00	2.24	1.27	0.45	1.39	57
3.	24.0	4300	20	16.4	2.52	1.47	0.00	0.78	58
4.	24.0	4500	0	0.00	2.54	0.68	0.03	1.07	27
σ					0.050	0.050	0.014	0.180	5

Table 3 UV intensity and power usage for the UV lamps used in the demonstration reactor

UV Lamp	Power Used by Lamp (watts)	Power Used by Ballast (watts)	UV @ 6.4 cm (mW/cm^2)	UV Power From Lamp** (watts)	UV Eff. (%)
Black-Light	20.1	1.15	2.4	4.2	16.5
Germicidal 1	22.4	0.98	4.9	8.3	26.2
Ozone	22.4	0.98	4.9*	8.3*	26.2

* UV at 254 nm

** $\text{UV} - \text{Power} = \dfrac{1.5\,\pi^2\, y\left(4y^2 + L^2\right)^{\frac{3}{2}} I_{UV}}{12y^2 + 2L^2}$ where L is the lamp length, y is the distance from the lamp to the UV-meter, I_{UV} is the UV intensity at y.

Table 4 DMMP disappearance with photocatalytic titania, effects of UV-lamp and flow rate: oxygen at 20%

#	Lamp*	Flow Rate (lpm)	Water Vapor (ppm)	Ozone (ppm)	DMMP (ppm)	ΔDMMP (ppm)	ΔCO_2 (ppm)	ΔCO (ppm)	Eff. (%)
1.	Ozone	12.1	5200	33.0	1.74	1.74	---	---	100
2.	Germ.	12.1	5200	0.00	2.03	1.48	1.13	1.27	73
3.	Black-Light	12.1	5400	0.00	2.03	0.72	0.90	0.69	35
4.	Ozone	24.0	3800	16.4	2.33	2.33	---	---	100
5.	Germ.	24.0	3900	0.00	2.33	0.99	1.29	1.10	42
σ					0.050	0.050	0.014	0.180	5

* Test # 6 used two UV lamps, all other tests used a single UV lamp

Theory-Experiment Comparisons

A one-dimensional computerized model of photocatalytic reactors was previously presented by Hall et al. [7] for honeycomb monoliths. The program is based on analysis of the distribution of UV light within diffusely illuminated honeycomb channels using conventional shape factor analysis, mass transfer of gaseous contaminants to the channel surfaces using standard one-dimensional Sherwood number correlations, and photocatalytic destruction of the contaminants on the surface using measured intrinsic destruction rates. Comparisons of the model predictions with experiments performed in a demonstration reactor are shown in [7] to be quite good for contaminants such as formaldehyde and toluene.

The model deals only with heterogeneous, photocatalytic destruction of DMMP, with no gas-phase chemistry included. Therefore, only those experiments which used either black- or germicidal lamps and for which the destruction could be attributed to photocatalytic processes were modeled. The intrinsic rate and UV intensity dependence measured for DMMP were used. The mini-reactor tests were conducted at relative humidity levels close to that for which the intrinsic rate was measured, and no further corrections for relative humidity were made. Although the intrinsic rate was measured with a black-lamp, it was assumed that there is no difference between black- and germicidal lamps on a unit UV flux basis.

Table 5. Comparison of Theory with Experiments

Experiment	**Flow rate (lpm)**	DMMP Conc. (ppm)	UV Flux (mW/cm^2)	Measured Efficiency	Calculated Efficiency
2	12.1	1.74	4.9	68%	60-67%
3	12.1	2.03	4.9	73%	60-66%
4 *	12.1	2.03	2.4	35%	43-50%
6 **	24.0	2.33	4.9	42%	46-53%

* Black-light
** Two UV lamps

Two calculated efficiencies are shown in Table 5. The lower of the two corresponds to a correction to the intrinsic rate for the possibility that the UV meter was out of calibration at the time the intrinsic rate measurement was made (the meter was found to be out of calibration about a year later in other tests with the real UV intensities a factor of 1.35 greater than indicated). The approach velocities corresponding to the two flow rates in Table 5 are so low (5 and 10 cm/sec) that mass transfer resistance is a significant influence in the experiments. The model is seen to be slightly low relative to experiment for tests 2 & 3, and higher than experiment for tests 4 & 6. However, given the simplicity of the model and experimental uncertainties, the agreement is encouraging, and gives support to the idea that the model could be used to design scaled-up reactors which could be used for large scale destruction of DMMP.

As an example, the predicted performance of a large scale reactor capable of purifying 200 CFM of air containing DMMP at 100 ppm is shown in Fig 12. The reactor consists of 12 titania-coated honeycomb monoliths spaced about 8 inches apart each with a cross-sectional area of 20 square feet. Using the slower of the two intrinsic destruction rates for DMMP discussed previously, the single pass efficiency of the device reaches 99.85% with a total input power of 18 kW. The gas would be heated about 50 deg C for this power input. For the faster of the two rates, the power consumption would be about 20 % less for the same efficiency.

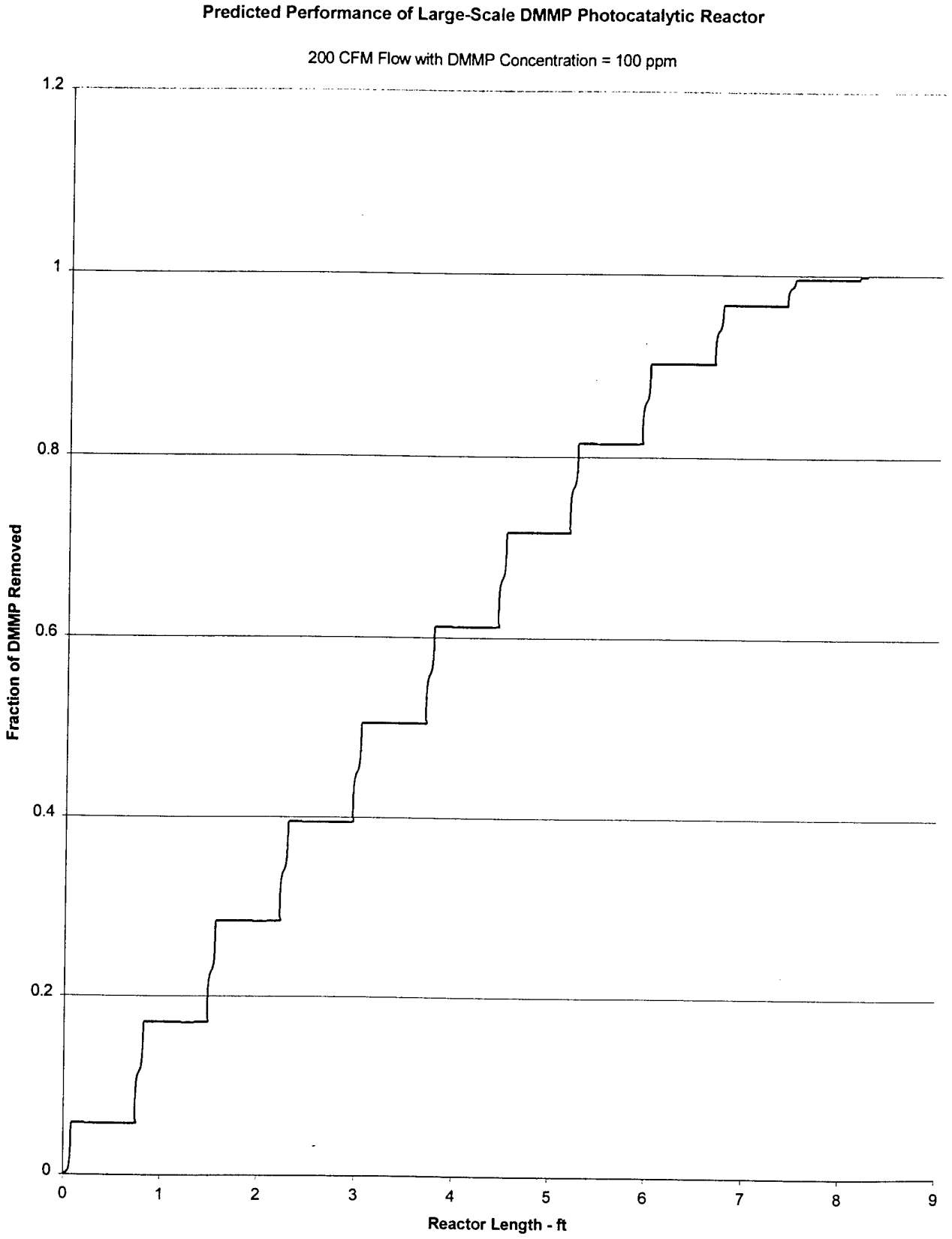

Fig 12 Predicted Performance of Large-Scale DMMP Photoreactor.

Conclusions

In summary, we believe that significant advances were made during the three year ARO contract on the photocatalytic and thermocatalyltic decomposition of the CWA simulant, DMMP. The most important result during the final year of the contract was the discovery of catalysts (primarily V on silica) that exhibited high conversion (~99.9% conversion to our detection limit of 0.1%) of DMMP. The catalysts were run continuously for over 100 hours with no apparent deactivation. Various characterization methods were employed to elucidate the mechanism and it was found that P_2O_5 plays an important catalytic role, instrumental in maintaining high conversion of DMMP for prolonged periods. Activated carbon was also found to be effective in destroying DMMP at temperatures above 673 K, with no deactivation- once again due to P_2O_5 formation. In addition to the thermocatalytic study, a photocatalytic reactor prototype was constructed for the destruction of DMMP using titania as the catalyst. The reactor was designed based on intrinsic rate measurements done at UTRC and a model developed previously at UTRC for titania-coated honeycomb monoliths. The experimental conversion efficiencies were in reasonable agreement with those predicted by the model. An approximate reactor size is given based on 99.85% conversion efficiency of DMMP. Although photocatalysis is a widely publicized method, it is important to consider the fact that catalyst poisoning does occur. It is therefore important to include kinetic rates and detailed modeling, such as the work begun in this study, before developing prototype systems for the military.

Future work in this area, potentially through a follow-on proposal submitted in '99, would benefit by a 'combinatorial' or 'high-throughput screening' approach to further develop and optimize catalysts for efficient destruction of CWA simulants.

References:

1. Lee; K. Y.; Houalla, M.; Hercules D. M.; Hall W. K. *J. Catal.* **1994**, *145*, 223-231.
2. Graven, W. M.; Weller, S. W.; Peters, D. L. *Ind. Eng. Chem. Process Des. Dev.* **1966**, *5*, 183-189.
3. Mitchell, M. B.; Sheinker, V. N.; Mintz, E. A. *J. Phys. Chem.* B **1997**, *101*, 11192-11203.
4. Thomas, L.C.; Chittenden, R. A. *Spetrochim. Acta.* **1964**, *20*, 467-487.
5. Corbridge, D. E. C.; Grayson, M. and Griffith E. J., Eds., *Topics in Phosphorus Chemistry*, Vol. 5 Interscience, New York, **1969**, p. 275.
6. Baier, R. W.; Weller S. W. *Ind. Eng. Chem. Process Des. Dev.* **1967**, *6*, 380-385.
7. Hall, R. J., Bendfeldt, P., Obee, T. N., and Sangiovanni, J. J., "Computational and Experimental Studies of UV/Titania Photocatalytic Oxidation of VOC's in Honeycomb Monoliths", *Journal of Advanced Oxidation Technologies*, Vol. 3, No. 3, p. 243, 1998.

(5) TECHNOLOGY TRANSFER:

Patent disclosures filed as discussed in (3). No other technology transfer but discussions were held with UTC Business Units and at Aberdeen.

APPENDIX

(Reprints)

Reprinted from

Journal of
Photochemistry
and
Photobiology
A: Chemistry

Journal of Photochemistry and Photobiology A: Chemistry 118 (1998) 45–51

Photocatalytic decomposition of DMMP on titania

Timothy N. Obee, Sunita Satyapal*

United Technologies Research Center, 411 Silver Lane, East Hartford, CT 06108, USA

Received 22 December 1997; received in revised form 20 April 1998; accepted 4 August 1998

ELSEVIER

JOURNAL OF PHOTOCHEMISTRY AND PHOTOBIOLOGY A: CHEMISTRY

Types of Contribution
Original papers not previously published. – Preliminary notes. – Reviews.

Papers and Reviews may be concerned with either quantitative or qualitative aspects of photochemistry. Organic, inorganic and coordination systems are all treated. The scope includes the physical chemistry of excited atoms or molecules, studies of electronic energy transfer, quantum yield determinations and kinetic measurements made under stationary or non-stationary conditions, measurements of rate constants for primary or secondary photochemical processes, studies of absorption or emission spectroscopy applied to photochemistry, mechanistic investigations of photochemical reactions based on product analysis or energy transfer studies, identification of the products of photochemical reactions, and studies related to the photochemical conversion and storage of solar energy and to atmospheric photochemistry. Papers relating to Applied Photochemistry are also published. This field includes studies of photoinitiation of polymerization, photo-cross-linking, photodegradation or photostabilization of polymers, photohalogenation, chemical aspects of photography and the design of photoreactors.

Preliminary Notes will describe work that is not yet completed, but that needs, for some reason, to be published in its preliminary form. Manuscripts submitted for consideration in this category must be accompanied by a reasoned justification of the need for urgent publication. This justification will be used by the Editors in deciding whether preliminary publication should be permitted, or whether the authors should be asked to submit a full paper when their research is completed.

Review articles are occasionally published, and suggestions of suitable topics are welcomed. Prospective authors should, however, discuss the content and length of a proposed review before embarking on its preparation.

Frequency
Ten volumes per year.

Subscription Information 1998
Volumes 112–121, each volume containing 3 issues, are scheduled for publication. Prices are available from the publishers upon request. Subscriptions are accepted on a prepaid basis only. Issues are sent by SAL (Surface Air Lifted) mail wherever this service is available. Airmail rates are available upon request.

Orders, claims and product enquiries
(no manuscript enquiries)

Please contact the Customer Support Department at the Regional Sales Office nearest you:

New York
Elsevier Science
P.O. Box 945
New York, NY 10159-0945, USA
Tel.: (+ 1) 212-633-3730
[Toll free number for North American customers: 1-888-4ES-INFO (437-4636)]
Fax: (+ 1) 212-633-3680
E-mail: usinfo-f@elsevier.com

Amsterdam
Elsevier Science
P.O. Box 211
1000 AE Amsterdam
The Netherlands
Tel.: (+ 31) 20-4853757
Fax: (+ 31) 20-4853432
E-mail: nlinfo-f@elsevier.nl

Tokyo
Elsevier Science
1-9-15 Higashi-Azabu 1-chome
Minato-ku, Tokyo 106-0044
Japan
Tel.: (+ 81) 3-5561-5033
Fax: (+ 81) 3-5561-5047
E-mail: info@elsevier.co.jp

Singapore
Elsevier Science
No. 1 Temasek Avenue
#17-01 Millenia Tower
Singapore 039192
Tel.: (+ 65) 434-3727
Fax: (+ 65) 337-2230
E-mail: asiainfo@elsevier.com.sg

Rio de Janeiro
Elsevier Science
Rua Sete de Setembro 111/16 Andar
20050-002 Centro
Rio de Janeiro - RJ, Brazil
Tel.: (+ 55) (21) 509 5340
Fax: (+ 55) (21) 507 1991
E-mail: elsevier@campus.com.br

[Note (Latin America): for orders, claims and help desk information, please contact the Regional Sales Office in New York as listed above]

ELSEVIER

Journal of Photochemistry and Photobiology A: Chemistry 118 (1998) 45–51

Journal of Photochemistry and Photobiology A:Chemistry

Photocatalytic decomposition of DMMP on titania

Timothy N. Obee, Sunita Satyapal*

United Technologies Research Center, 411 Silver Lane, East Hartford, CT 06108, USA

Received 22 December 1997; received in revised form 20 April 1998; accepted 4 August 1998

Abstract

The photocatalytic decomposition of gas-phase dimethyl methylphosphonate (DMMP) on TiO_2-coated glass substrate was studied using a single-pass reactor. The disappearance of DMMP and the appearance of products were monitored for several DMMP concentrations between 1 and 90 ppmv in air. Intrinsic reaction rates were determined, products were identified and reaction chemistry has been postulated. The main reaction products identified were carbon dioxide and carbon monoxide in the gas-phase, and methylphosphonic acid and phosphate on the catalyst. It was found that due to build-up of surface phosphorus-containing species, the catalyst de-activated relatively rapidly. One of the interesting results of this study is that the catalyst activity was completely recovered by washing with water and partially recovered by exposure to UV (UVA; ~ 352 nm) light.

Keywords: DMMP; Titania; Photocatalysis; Organophosphorus; Photo-oxidation; Nerve gas

1. Introduction

The decomposition of organophosphorus compounds has been of interest for several years, primarily for the destruction of chemical warfare agents and pesticides, as well as other phosphorus-containing hazardous waste. With approximately 25 000 tons of chemical weapons stockpiled in the US alone, there is interest in developing methods alternate to incineration for safely destroying these stockpiles. In addition to large-scale disposal, destroying trace quantities of such pollutants in enclosed spaces is important for storage and transport applications. Photocatalysis has emerged over the last two decades as a low cost and environmentally benign method to destroy low concentrations of pollutants in air and aqueous feed streams. In this study we report the photocatalytic oxidation of dimethyl methylphosphonate (DMMP); a widely used simulant for nerve gas (e.g., iso-propyl methylphosphonofluoridate or GB).

One of the main difficulties in the catalytic decomposition of phosphorus-containing compounds is poisoning or degradation of the catalyst. Several studies have been reported on the thermal decomposition of DMMP on various substrates, including Ni (1 1 1), Pd (1 1 1), Rh (1 0 0), Al_2O_3, Mo (1 0 0), Fe_2O_3, SiO_2, and Pt [1–8]. In most of the above studies, with the exception of Mo (1 0 0), the catalytic reaction was not sustained due to the accumulation of products on the catalyst surface. In contrast to the thermally catalyzed reactions of DMMP reported above, we have studied the photocatalytic decomposition of DMMP on titania at room temperature. The use of titania for the oxidation of organophosphonates and pesticides in aqueous solutions has been documented in recent studies [9–15]. As opposed to liquid-phase reactions, we report here the photocatalytic reaction of DMMP in the gas-phase on a titania-coated glass support. The goals of the study were to determine intrinsic oxidation rates, identify reaction products, and demonstrate rejuvenation of the de-activated catalyst.

2. Experimental

2.1. Materials

DMMP was purchased from Aldrich and used without further purification. Titania, P-25 was purchased from Degussa. Nitrogen from an in-house source and oxygen (Matheson; 99.999%) were used in all experiments.

2.2. Intrinsic rate apparatus

A glass-plate photocatalytic reactor was used to generate intrinsic oxidation rate data. A complete description of the reactor and its operation is presented elsewhere [16]. Ultraviolet (UV) illumination was provided by a pair of black-

*Corresponding author. Tel.: +1-860-610-7378; fax: +1-860-610-7911; e-mail: satyaps@utrc.utc.com

1010-6030/98/$ – see front matter
PII: S1010-6030(98)00372-4

light lamps (352 nm peak intensity, SpectroLine XX-15A). UV-intensity at the catalyst surface was measured by a UVA power meter (Oriel UVA Goldilux). DMMP was generated by vaporizing DMMP in a temperature-controlled-water bath. Control of the DMMP generation rate was effected through selection of the water bath temperature and the length and diameter of a feed tube leading from a DMMP containment vial; the DMMP effluent from the vial was swept away by a flow of nitrogen gas. High-purity nitrogen gas passed through a water bubbler to set the desired water vapor level. An oxygen gas flow was combined with the nitrogen and DMMP flows to produce the desired carrier gas mixture (10% oxygen and 90% nitrogen).

An opaque film of Degussa P-25 titania was deposited on flat 25 mm wide microscope glass slides using a wash-coat process. The wash-coat was 5% by weight of titania in distilled water. A titania film was prepared by dipping the glass slide in the wash-coat several times, air-dried between dippings, and then oven-dried at 60°C. This process was repeated until a 0.90 mg/cm^2 film (one side) was attained. A fresh titania-coated slide was used in each DMMP experiment. The photocatalytic activity of each catalyst slide was determined from the photo-oxidation of 1-butene, which has been previously studied in this laboratory.

2.3. Analysis of reaction products

The concentrations of water vapor, carbon dioxide, and carbon monoxide were measured using a photo-acoustic detector (Brüel and Kjær 1302). The concentrations of DMMP and 1-butene were measured using a gas chromatograph (HP-5890 II) equipped with an FID detector and a megabore column (Restek RTX-502.2). Gas standards (Matheson) were used to calibrate the detectors for carbon dioxide, carbon monoxide, and 1-butene. A standard for DMMP was provided by vaporizing DMMP in a temperature-controlled oven (Metronics 230 Dynacalibrator). Formaldehyde and methanol were not detectable with the photo-acoustic detector due to overlap of DMMP absorption bands in the IR region.

After reaction with DMMP, the titania slides were immersed in distilled deionized water and the reaction products were extracted using ultrasonication. The extracted products were analyzed by ion chromatography using a Dionex AS4A-SC anion exchange column and a Na_2CO_3/$NaHCO_3$ buffer. Standards of methyl phosphonic acid (MPA) and phosphate (phosphoric acid) were used to identify the products.

In order to collect gas-phase products, a cold-trap (dry ice/acetone at ~−78°C or ethanol/liquid nitrogen maintained at ~−80°C) was used to trap volatile products at the exit of the titania reactor. The concentrated products were then identified by GC/GCMS/IR. The primary gas-phase products that we attempted to detect with the mass-spectrometer included methanol, formaldehyde, formic acid, and methyl formate.

3. Results and discussion

3.1. Preliminary reactivity measurements

Control experiments verified that under UV-illumination, no change in DMMP level or evolution of carbon dioxide or carbon monoxide was observed with uncoated slides. It was also shown that both oxygen and UV-light were required for photocatalytic decomposition of DMMP on TiO_2. There was no significant loss of DMMP due to adsorption/reaction on non-catalytic surfaces in the apparatus.

In a study of film loading by Jacoby et al. [17], the oxidation rate of trichloroethylene increased with film loading up to a titania (Degussa P-25) loading of 0.5 mg/cm^2 and remained constant for all higher loadings. This finding suggested that the oxidation rate maximized at a film loading of 0.5 mg/cm^2 and that additional film loading added nothing to the oxidation rate. This conclusion should not depend on the specific contaminant used, and hence, can be applied in the present study. The titania film in the present study was determined to be opaque to UVA by placing a coated plate between the UV black-light lamps and the UVA power meter. This finding coupled with the conclusion drawn from Jacoby et al's. finding [17] suggested that the UV-radiation was being maximally utilized in the oxidation process reported herein.

Oxygen was maintained at a constant level of 10% by volume for all rate measurements. Jacoby et al. [17] and Dibble and Raupp [18] have found that for the oxidation of trichloroethylene the rate was zero-order for oxygen levels above 1%. In view of the reported findings, and since the experiments performed in the present study used contaminant levels that were lower than the levels used by Jacoby et al. [17] and Dibble and Raupp [18], it is likely that the oxidation rates herein were independent of oxygen level for oxygen levels above 1%.

3.2. DMMP oxidation rates

For the data generated with the glass-plate reactor, the oxidation rate was defined as

$$r = 2.45(X_{in} - X_{out})Q/A \quad (1)$$

where r (μ mol/cm^2 h) is the oxidation rate, X_{in} (ppmv) and X_{out} (ppmv) are the inlet and outlet contaminant (DMMP or 1-butene) concentrations, respectively, Q (lpm), the volumetric flow rate, and A (cm^2), the area of the titania-coated glass-plate; the numerical coefficient accounts for the units change.

Intrinsic rate determinations were performed at a 4 lpm flow rate. To check for gas-side mass-transfer influence, the flow was doubled to 8 lpm. The subsequent oxidation rate remained unchanged indicating that the oxidation rates obtained at the 4 lpm flow were free of gas-side mass-transfer influence [19].

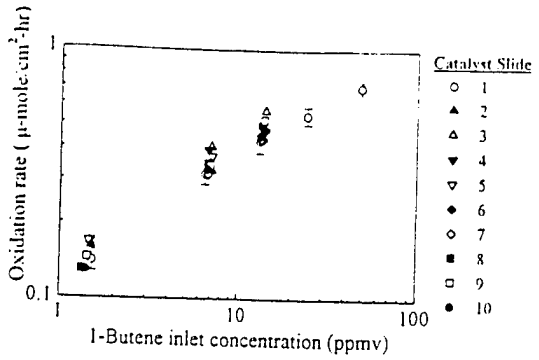

Fig. 1. Variance in photocatalyst activity of separate catalyst slides using 1-butene photo-oxidation: 1.96 mW/cm^2 UV; 5700 ppmv humidity.

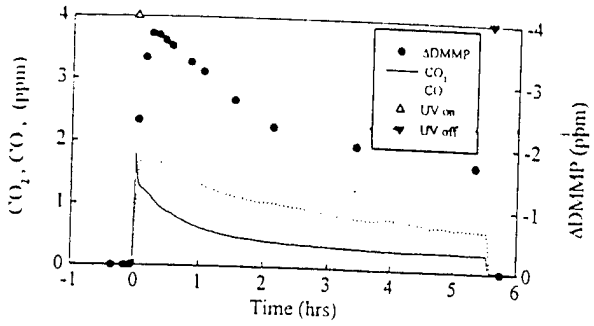

Fig. 3. Photo-oxidation of DMMP: UVA 1.96 mW/cm^2; water vapor 5700 ppm; 48 ppm DMMP influent.

The relative fractional change in the DMMP (or 1-butene) concentration through the reactor was maintained below 0.1 through the selection of an appropriate catalyst (slide) length. This ensured that the reactor was being operated in a differential mode during rate determinations.

In all photo-oxidation experiments the following protocol was used: first, the gas flows and water vapor levels were set. After the reactor inlet/outlet water vapor levels reached equilibrium, DMMP (or 1-butene) was introduced. When the inlet/outlet DMMP (or 1-butene) concentration reached steady-state and was of equal magnitude, the UV-lamp was illuminated.

As discussed below, the photo-oxidation of DMMP resulted in the deactivation of the catalyst. As a result, a new titania-coated slide was used in each DMMP experiment. Prior to most DMMP experiments, the photo-activity of the subject catalyst slide was first determined by the photo-oxidation of 1-butene at several 1-butene influent concentrations. A sample of the resultant 1-butene rate determinations is shown in Fig. 1, in which each symbol in Fig. 1 represents a distinct slide allocated for a subsequent DMMP experiment. A variance of about 5% in the relative 1-butene oxidation rate was found from all the slides so far examined. Catalyst de-activation by 1-butene was not observed in any long-term exposure, as shown, for example, in Fig. 2. Importantly, in repeat DMMP experiments, the same DMMP result of oxidation rate dependence with time was found whether or not the subject catalyst was previously exposed to 1-butene.

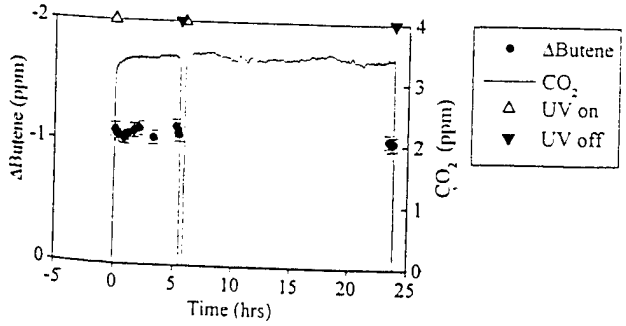

Fig. 2. Stability of 1-butene photo-oxidation: UVA 0.94 mW/cm^2, 13.9 ppm 1-butene influent, 5500 ppm water vapor.

Evidence for DMMP photocatalytic oxidation is shown in Fig. 3. A decrease in the reactor DMMP effluent, that is, a negative DMMP differential change (ΔDMMP in Fig. 3) through the reactor, was seen after the UV-lamp was illuminated. Concomitant with the decrease in DMMP concentration was the appearance of CO_2 and CO. After the UV-lamp was extinguished, ΔDMMP, CO_2, and CO returned to zero. The appearance of ΔDMMP when the UV-lamp was illuminated was interpreted as a photo-oxidation process. A carbon balance of the moment the UV-lamp was extinguished indicated that only about 20% of the carbon was being released as gas-phase CO_2 and CO.

At a relatively high UV-irradiation, a high initial rate of catalyst de-activation was seen following the activation of the UV-lamp, but which decreased as the influent DMMP was decreased (Fig. 4(A)). At the highest DMMP inlet concentrations in Fig. 4, catalyst de-activation was evident when the UV-exposure was observed over a time interval as short as a few hours following the activation of the UV-lamp. At a lower UV-irradiation, the catalyst de-activation rate was also lowered (Fig. 4(B)).

The oxidation rate, defined by Eq. (1), was considered meaningful when the adsorbate, DMMP, was in equilibrium with its gas-phase. If the oxidation process had reached a steady-state, then such a state of equilibrium would indeed exist. If stringently applied, the requirement of a state of equilibrium was not reached with DMMP, since the oxidation of DMMP de-activated the titania catalyst. However, if the rate of catalyst de-activation was sufficiently slow, then a pseudo steady-state of equilibrium may be envisioned to exist, and the oxidation rates may then be considered dependent, as an approximation, on the attendant DMMP gas-phase concentration.

The photocatalytic oxidation of gaseous contaminants on titania was shown to follow Lagmuir–Hinshelwood (L–H) kinetics in many studies [16,18,20–24]. L–H kinetics expresses a dependent relationship between the oxidation rate of a contaminant and its attendant gas-phase concentration, and furthermore, requires that a state of equilibrium exists between the adsorbate (i.e., contaminant) and its gas-

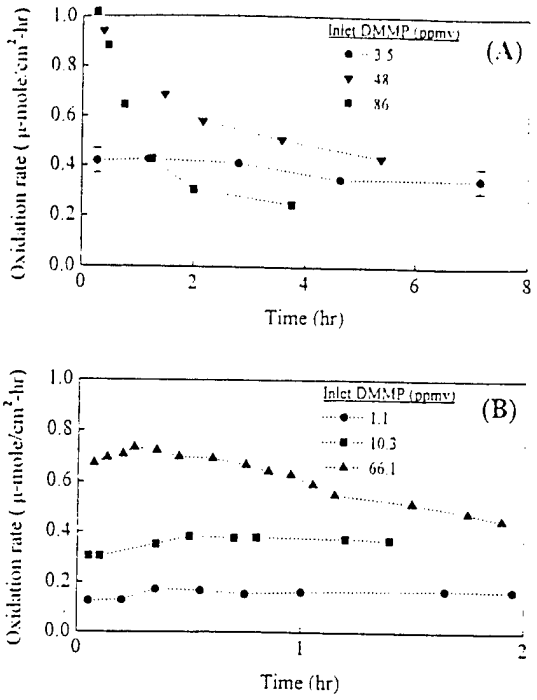

Fig. 4. Influence of DMMP concentration on catalyst de-activation (UV-lamp activated at 0 h): (A) 1.96 mW/cm^2 UV, 5700 ppmv humidity; (B) 0.94 mW/cm^2 UV, 5600 ppmv humidity.

phase [25]. To examine if the DMMP rate data followed a L–H rate form, an initial oxidation rate, defined herein as the highest measured oxidation rate at a given influent DMMP concentration, was used for the dependent variable.

A pseudo steady-state condition was likely to be achieved in Fig. 4(B) and for the lowest DMMP concentration in Fig. 4(A). The existence of a pseudo steady-state may not have been reached for the two highest DMMP concentrations in Fig. 4(A), and subsequently, the initial oxidation rate, as a pseudo steady-state oxidation rate, would be poorly determined. The initial oxidation rates computed from the data in Fig. 4 are shown in Fig. 5. Included in Fig. 5, was a fit to a unimolecular L–H rate form [25] for the low UV-irradiation (0.94 mW/cm^2) case. An adequate L–H fit was possible through the lower DMMP concentrations. It was not

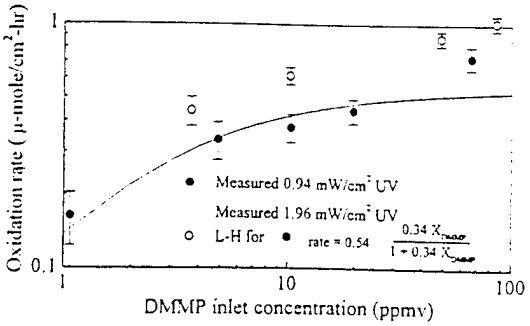

Fig. 5. Influence of DMMP concentration on DMMP initial oxidation rate: (●) 0.94 mW/cm^2 UV; (○) 1.96 mW/cm^2 UV; all data at 5700 ppmv humidity.

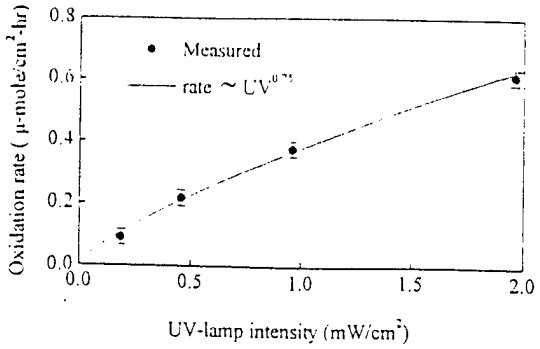

Fig. 6. Influence of UVA irradiation on DMMP initial oxidation rate: 8.1 ppmv DMMP inlet, 6000 ppmv water vapor.

possible to also include the highest DMMP concentration, and it may be the result of not having achieved the pseudo steady-state condition, as discussed above.

The influence of UV-irradiation on DMMP initial oxidation rate is shown in Fig. 6. A low DMMP inlet concentration was used so that a pseudo steady-state rate could be established. The functional dependence of the oxidation rate on UV- intensity is well established both experimentally and theoretically [18,24,26], that is, UV-intensity raised to a power. The result (exponent in Fig. 6) is in agreement with those found by others [22,27] under similar UV-intensities.

3.3. Regeneration of depleted titania

One of the most interesting results of our study is that a de-activated titania catalyst may be easily regenerated by washing with water or by subjecting the catalyst in situ to UV-light in the absence of DMMP. The effect of these two regeneration strategies is shown in Fig. 7. The data shown in Fig. 7 was generated in a particular chronological order. First, a recently titania- coated slide was exposed to UV-illumination, following the stated experimental protocol, and allowed to de-activate (Fig. 7(A)). Next, the slide was exposed in situ to UV-light for 12 h in the absence of DMMP. Following this re-conditioning period, the slide was once again exposed to DMMP (Fig. 7(B)). By comparing Fig. 7((A) and (B)) some catalyst rejuvenation was achieved. This rejuvenation most likely resulted from oxidation of adsorbed DMMP and photodesorption of the adsorbed intermediates during the reconditioning period. The presence of adsorbed intermediates has been suspected to be a root cause of the titania catalyst deactivation [22]. The slide was then kept in the dark for 12 h in the absence of DMMP as another potential rejuvenation means. Following this reconditioning period, the slide was once again exposed to DMMP (Fig. 7(C)). A comparison of Fig. 7((B)and (C)), indicated that catalyst rejuvenation was not achieved, however. Next, the slide was removed, washed in distilled water (sequentially dipped in four fresh cylinders of distilled water and dried at approximately 35°C for roughly 10 min), and returned to the reactor. The slide was once again exposed to DMMP (Fig. 7(D)). A comparison of Fig. 7((A) and (D))

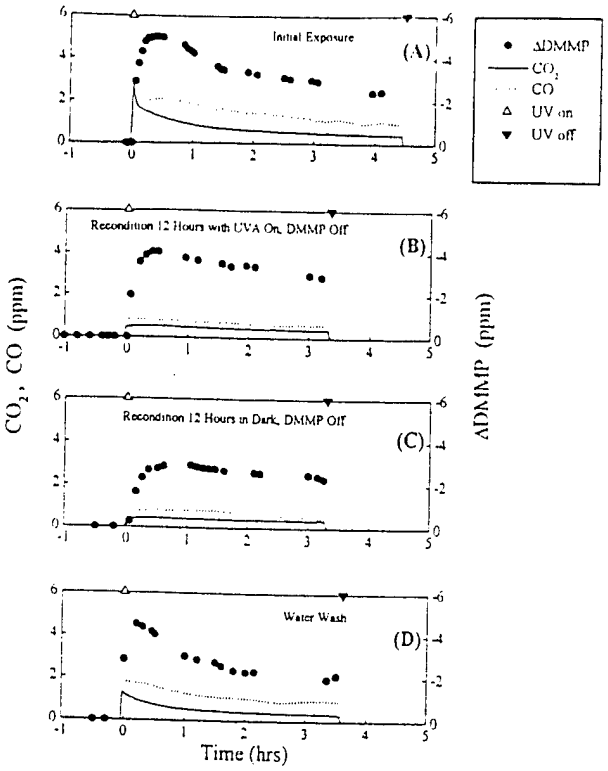

Fig. 7. Effect of catalyst regeneration strategies: water vapor 5700 ppm, 60 ppm DMMP influent; (A) initial exposure, UVA 0.94 mW/cm^2; (B) re-condition by 12 h with UVA on, DMMP off; (C) re-condition by 12 h in the dark, DMMP off; (D) re-condition by water wash.

indicated that catalyst rejuvenation was again achieved. The water wash and the UV-exposure rejuvenation strategies were repeated, but instead of exposing the catalyst to DMMP as a test for rejuvenation, the catalyst was exposed to 1-butene and UV-illumination. The crucial comparison was between the oxidation rate of 1-butene determined on a new titania-coated slide against the oxidation rate of 1-butene on the supposed rejuvenated slide. Again, the water wash strategy was found to completely rejuvenate the catalyst, while a 2 h exposure to UV-irradiation was found to partially rejuvenate the catalyst.

The washing of titania with water, as opposed to drying at 35°C, is believed to be responsible for rejuvenating the catalyst. Previous studies have shown that temperatures greater than 100°C are required to remove adsorbed water from the surface of titania [28]. This is due to the fact that the surface of the titania in a humid environment is hydroxylated and contains adsorbed water and hydroxyl groups. Water strongly adsorbs on the hydroxylated titania surface via hydrogen bonding to surface hydroxyl groups [28]. Other molecules that are also strongly bonded to the surface hydroxyl groups of hydroxylated anatase and rutile, via hydrogen bonding, include phenol, ammonia and pyridine [29]. In addition, adsorption on a dehydroxylated site can result in irreversible chemisorption [30]. Creation of a dehydroxylated site can result from the oxidation reaction itself. In the case of DMMP, methyl phosphonic acid and phosphate, strong adsorption to the hydroxylated titania surface may take place via the phosphorus atom, and/or via the oxygen atom of either methoxy or hydroxyl groups. The low vapor pressures of these compounds also suggests that they remain on the de-activated catalyst during the brief, low temperature drying process.

3.4. Reaction pathways

The molecular structures of the nerve gas sarin (GB) and the simulant DMMP are shown below.

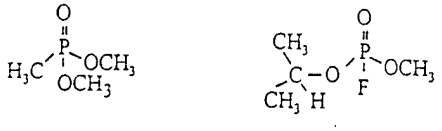

DMMP Sarin

The decomposition of DMMP compared to nerve gas is predicted to be more difficult due to the absence of fluorine atoms which may act as a better leaving group than methyl or methoxy radicals.

Several recent studies in the literature are relevant to the results we report here [9–15]. Tanaka and co-workers, for example, have recently investigated the photocatalytic degradation of the insecticides DDVP (dimethyl-2,2-dichlorovinyl phosphate) and DEP (dimethyl-2,2,2-trichloro-1-hydroxyethyl phosphonate) in aqueous suspensions of TiO_2 [14]. The main products observed were Cl^- and PO_4^{3-}, with formaldehyde as an intermediate that disappeared under further reaction. In a study by Fox and co-workers [13], butylphosphonic acid, benzylphosphonic acid and phenylphosphonic acid were decomposed in aqueous TiO_2 suspensions. Kinetic data were found to be consistent with a Langmuir–Hinshelwood model [13].

According to the generally reported mechanism for photocatalytic decomposition using TiO_2, irradiation of TiO_2 promotes a valence band electron to the conduction band ([13,26] and references therein). This results in a conduction band electron (e_c^-) available for reducing species on the surface of the semiconductor, and a valence band hole (h_v^+) capable of oxidizing species adsorbed on the substrate. The actual mechanism of oxidation/reduction, is believed to involve the production of superoxide anions and hydroxide radicals as shown in Eqs. (3) and (4).

$$TiO_2 + h\nu \rightarrow e_c^- + h_v^+ \quad (2)$$

$$e_c^- + O_2 \rightarrow O_2^- \quad (3)$$

$$h_v^+ + H_2O \rightarrow H^+ + {}^{\bullet}IOH \quad (4)$$

The conduction band electron, e_c^-, is believed to be trapped by adsorbed O_2 to form a superoxide ion (Eq. (3)). The valence band hole, h_v^+, may be trapped by H_2O to form OH radicals; or by an adsorbed organic (e.g., DMMP or phophonate intermediates) as discussed in the literature [13,31,32].

In Fox's study [13], evidence was found for cleavage of the carbon–phosphorus bond and a postulated mechanistic

route was reported as shown in Eq. (5).

$$\phi\text{–}CH_2\text{–}P(=O)(OH)_2 + H_2O + h_v^+ \rightarrow \phi\text{–}CH_2^{\bullet} + H_3PO_4 + H^+ \quad (5)$$

The benzyl radical was found to be an intermediate for the observed species ϕ–CH_2OH, ϕ–CHO, and ϕ–CH_2CH_2–ϕ. In our study, we believe that the more common route of P–O cleavage occurs before eventual P–C cleavage. This is due to the observance of methyl phosphonic acid, CH_3–$P(=O)(OH)(OCH_3)$. We also observed phosphate (PO_4^{3-}) and CO_2, indicative of complete oxidation of DMMP.

In addition to direct oxidation by valence band holes as discussed above, hydroxyl radical attack provides another oxidation pathway for DMMP. The primary mechanisms for the photocatalytic oxidation of DMMP via hydroxyl radical attack, are hydrogen abstraction and addition–elimination [11]. Further oxidation to produce CO/CO_2 and H_2O from methanol and formaldehyde is anticipated as a result of the high reactivity of these compounds on titania. A previous investigation of the photocatalytic oxidation of DMMP in an aqueous solution of titania [11] found that methanol was not observed, thereby suggesting that the addition–elimination mechanism is not significant under aqueous conditions. It is not possible at this time, to determine the importance of the hydroxyl radical mechanism as compared to the direct valence hole mechanism.

In our investigation, complete conversion of any methanol or formaldehyde that may be formed, to produce CO_2 and CO appears to be the dominant reaction. Phosphates remain on the surface along with methyl phosphonic acid which retains a portion of the carbon content of DMMP, thereby explaining the mass balance discrepancy based on gas-phase CO_2/CO alone. In contrast with the liquid-phase study [11], we have detected methyl formate ($HCOOCH_3$). Although, methyl formate may be formed directly on the TiO_2 surface, another possibility is the formation of methanol and formic acid which react readily to give methyl formate. We also observed methanol from a GC analysis of cold-trap constituents. The identification was based on the comparison of retention time with a methanol standard.

Hydrogen Abstraction

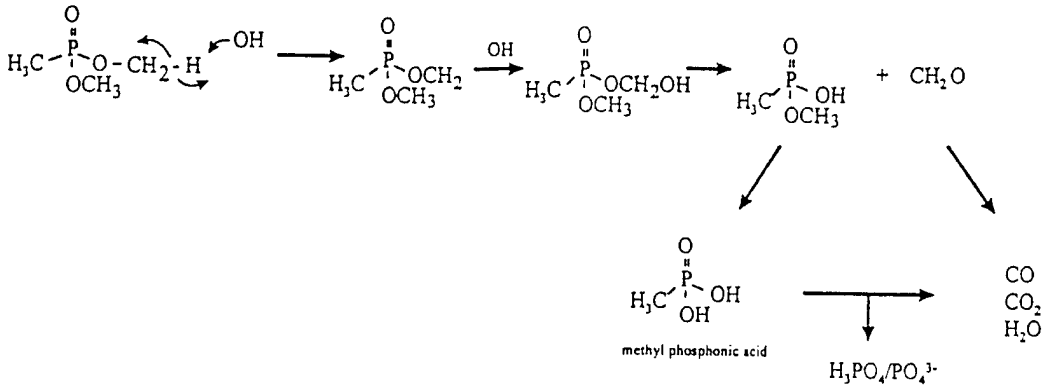

Addition - Elimination

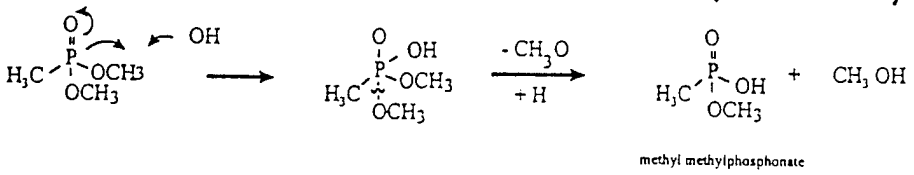

To investigate the formation of methyl formate, we injected a mixed gas-phase sample of formic acid and methanol into the GC–MS. The standard protocol of cryo-trapping to increase sensitivity was employed, and a GC–MS peak corresponding to methyl formate was observed. Therefore, any gas-phase methanol and formic acid may react during the process of detection via the GC–MS. In addition, methyl formate may be synthesized in the cold-trap during the process of collecting products from the titania reactor. It should also be noted that in the study of liquid-phase DMMP decomposition on titania, formic acid was detected as an intermediate, while neither methanol nor methyl formate were reported [11]. In contrast to the liquid-phase study which followed the accumulation of products over several days in a closed reactor [11], our reactor was not a batch system. The distribution of reactants, intermediates and products in equilibrium would therefore be different in both cases. It is also clear that in aqueous solution the role of water, acidity and basicity, and the ability to strip organic/inorganic phosphates from the surface of the catalyst, play a critical role.

4. Conclusions

In conclusion, we have determined the intrinsic rates for the photocatalytic decomposition of gas-phase DMMP on titania at room temperature. The products we detected were carbon dioxide, carbon monoxide, methylphosphonic acid and phosphate. There also appears to be methanol and methyl formate; the latter most probably originates from the reaction of methanol and formic acid. Finally, we have determined that washing of de-activated catalyst with water is sufficient for complete regeneration of the catalyst with respect to both DMMP and butene reactivity. The solubility of methyl phosphonic acid and phosphates in water aids in removing these species from catalytically active sites.

Acknowledgements

We would like to thank Dr. Xia Tang for her assistance with the ion chromatography detection and Dr. Dave Condit for helpful technical discussions. Work by Lisa Washmon, Mike Lindsay and Xiaodong Li in developing the GC–MS method is appreciated. Support for this work from the US Army Research Office, under contract DAAH04-96-C-0067, is gratefully acknowledged.

References

[1] X. Guo, J. Yoshinobu, J.T. Yates Jr., J. Phys. Chem. 94 (1990) 6839.
[2] R.I. Hegde, C.M. Greenlief, J.M. White, J. Phys. Chem. 89 (1985) 2886.
[3] M.K. Templeton, W.H. Weinberg, J. Am. Chem. Soc. 107 (1985) 97.
[4] M.K. Templeton, W.H. Weinberg, J. Am. Chem. Soc. 107 (1985) 107.
[5] V.S. Smentkowski, P. Hagans, J.T. Yates Jr., J. Phys. Chem. 92 (1988) 6351.
[6] M.A. Henderson, T. Jin, J.M. White, J. Phys. Chem. 90 (1986) 4607.
[7] W.M. Graven, S.W. Weller, D.L. Peters, Ind. Eng. Process Des. Dev. 5 (1966) 183.
[8] T.Z. Tzou, S.W. Weller, J. Catal. 146 (1994) 370.
[9] K. Harada, T. Hisanaga, K. Tanaka, New J. Chem. 11 (1987) 8.
[10] K.E. O'Shea, I. Garcia, M. Aguilar, Res. Chem. Intermed. 23 (1997) 325.
[11] K.E. O'Shea, J. Photochem. Photobiol. A: Chem. 107 (1997), 221.
[12] M.N. Schuchmann, Int. J. Radiat. Biol. 68 (1995) 121.
[13] K.W. Krosley, D.M. Collard, J. Adamson, M.A. Fox, J. Photochem. Photobiol. A: Chem. 69 (1993) 357.
[14] K. Harada, T. Hisanaga, K. Tanaka, Wat. Res. 24 (1990) 1415.
[15] J.J. Pignatello, Y. Sun, Wat. Res. 29 (1995) 1837.
[16] T.N. Obee, S.O. Hay, Environ. Sci. Technol. 31 (1997) 2034.
[17] W.A. Jacoby, D.M. Blake, R.D. Noble, C.A. Koval, J. Catal. 157 (1995) 87.
[18] L. Dibble, G. Raupp, Catal. Lett. 4 (1990) 345.
[19] C.G. Hill, An Introduction to Chemical Engineering Kinetics and Reactor Design, Wiley, New York, 1977, Chap. 6, pp. 178–181.
[20] T.N. Obee, R.T. Brown, Environ. Sci. Technol. 29 (1995) 1223.
[21] T.N. Obee, Environ. Sci. Technol. 30 (1996) 3578.
[22] J. Peral, D.F. Ollis, J. Catal. 136 (1992) 554.
[23] P. Pichat, J.-M. Herrmann, in: N. Serpone, E. Pelizzetti (Eds.), Photocatalysis: Fundamentals and Applications, Wiley, New York, 1989, chap. 8 and 18.
[24] A. Mills, S. LeHunte, J. Photochem. Photobiol. A: Chem. 108 (1997) 1.
[25] C.G. Hill, An Introduction to Chemical Engineering Kinetics and Reactor Design, Wiley, New York, 1977, pp. 182–184.
[26] D.F. Ollis, E. Pelizzetti, N. Serpone, Environ. Sci. Technol. 25 (1991) 1523–1529.
[27] S. Sitkiewitz, A. Heller, New J. Chem. 20 (1996) 233.
[28] G.B. Raupp, J.A. Dumesic, J. Phys. Chem. 89 (1985) 5240.
[29] B. Boddenberg, K. Eltzner, Langmuir 7 (1991) 1498.
[30] M. Nagao, Y. Suda, Langmuir 5 (1989) 42.
[31] C.K. Gratzel, M. Jirousck, M. Gratzel, J. Mol. Catal. 39 (1987) 347.
[32] M.T. Dulay, D. Washington-Dedeaux, M.A. Fox, J. Photochem. Photobiol. A: Chem. 61 (1991) 153.

Guide for Authors

Submission of Papers

Authors are requested to submit their manuscripts to

Editor-in-Chief: Professor R.P. Wayne
Physical and Theoretical Chemistry Laboratory
South Parks Road
Oxford OX1 3QZ
UK
FAX: +44 (1865) 275410
INTERNET: JPHOTO@Physchem.ox.ac.uk

Authors in the USA and Canada may submit their manuscripts to the North American Editor:

Professor R.P. Steer
Thorvaldson Building
University of Saskatchewan
110 Science Place
Saskatoon, SK
Canada S7N 5C9
FAX: +1 (306) 966 4730
INTERNET: STEER@SASK.USASK.CA

Authors in Asia should submit their manuscripts to the Asian Editor:

Professor H. Masuhara
Department of Applied Physics
Osaka University
2-1 Yamada-oka
Suita, Osaka 565
Japan
FAX: +81 6 876 8580

Contributions are accepted on the understanding that authors have obtained the necessary authority for publication. Submission of an article is understood to imply that the article is original and unpublished and is not being considered for publication elsewhere. Upon acceptance of an article by the journal, the author(s) will be asked to transfer the copyright of the article to the publisher. This transfer will ensure the widest possible dissemination of information.

Language

Papers will be published in English.
Authors in Japan please not that information about how to have the English of your paper checked corrected and improved (*before submission*) is available from: Elsevier Science Japan, Editorial Service, 1-9-15 Higashi Azabu, Minato-ku, Tokyo 106-0044, Japan; Tel: +81-3-5561-5032; Fax: +81-3-5561-5045; E-mail: info@elsevier.co.jp

Manuscript Preparation

Three copies of the manuscript should be submitted, in double-spaced typing on pages of uniform size with a wide margin on the left. Some flexibility of presentation will be allowed but authors are urged to arrange the subject matter clearly under headings such as Introduction, Experimental details, Results, Discussion, etc. References should be numbered consecutively (numerals in square brackets) throughout the text and collected together in a reference list at the end of the paper. Journal titles should be abbreviated according to the Chemical Abstracts Service Source Index, 1970 edition, and supplements. The abbreviated title should be followed by volume number, year (in parentheses) and page number.

Illustrations

Line drawings and cyclic or aromatic formulae should be in a form suitable for reproduction, drawn in Indian ink on drawing paper. They should preferably all require the same degree of reduction, and should be submitted on paper of the same size as, or smaller than, the main text to prevent damage in transit. Photographs should be submitted as clear black-and-white prints on glossy paper. Each illustration must be clearly numbered. "Quantity calculus" notation should be used for the labelling of the graph axes. Legends to the illustrations must be submitted in a separate list. All tables and illustrations should be numbered consecutively and separately throughout the paper.

Offprints

Offprints can be ordered at prices shown on the offprint order form.

Further Information

All questions arising after acceptance of a paper, especially those concerning proofs, should be directed to Elsevier Science Ireland Limited, Bay 15 K, Shannon Industrial Estate, Shannon, County Clare, Ireland (Tel.: +353 (61) 471 944; Fax: +353 (61) 472 144; E-mail: postmaster@elsevier.ie). The full and complete Instructions to Authors can be found on the World Wide Web: access under http://www.elsevier.nl or http://www.elsevier.com.

Photoassisted Decomposition of Dimethyl Methylphosphonate over Amorphous Manganese Oxide Catalysts

Scott R. Segal[†] and Steven L. Suib*[,†,‡,§]

U-60, Department of Chemistry, Department of Chemical Engineering, and Institute of Materials Science, University of Connecticut, Storrs, Connecticut 06269-4060

Xia Tang[∥] and Sunita Satyapal[⊥]

United Technologies Research Center, 411 Silver Lane, East Hartford, Connecticut 06108

Received September 22, 1998. Revised Manuscript Received April 22, 1999

The gas-phase decomposition of dimethyl methylphosphonate (DMMP) has been studied over amorphous manganese oxide (AMO) catalysts in the presence of light (~200−800 nm). The reaction was studied under oxidizing conditions using air at low temperatures (40−70 °C). DMMP and gas-phase products were studied using gas chromatography (GC). DMMP was found to adsorb strongly to the AMO surface and produce small amounts of methanol (MeOH) even in the absence of light. When AMO was irradiated with light of ~200−800 nm, large amounts of MeOH and CO_2 were initially formed. Following the initial period of high activity, strong deactivation was observed. After the reactions were performed, aqueous extracts from spent AMO were analyzed using ion chromatography (IC). The IC analyses indicated that several products accumulate on the AMO surface. These products include methyl methylphosphonate (MMP) and methylphosphonic acid (MPA). Greater amounts of MMP and MPA are produced after irradiation. Fourier transform infrared (FTIR) spectroscopy was used to examine adsorbed DMMP species on spent AMO. The IR results indicate that DMMP bonds to Mn Lewis acid sites on the AMO surface via the phosphoryl oxygen. On the basis of these results a mechanism is proposed for the adsorption and photoassisted decomposition of DMMP over AMO.

I. Introduction

There is current interest in developing new methods to safely destroy chemical warfare agents (CWAs). Such materials consist of extremely toxic organophosphorus nerve and blistering agents, including Soman (GD), Sarin (GB), and VX. The testing of CWAs in the laboratory is quite hazardous; therefore, studies are typically done using nontoxic simulants such as dimethyl methylphosphonate (DMMP).[1−11] The structure of DMMP is shown in Figure 1. DMMP is a liquid at 298K, having a low vapor pressure (1.05 Torr).[1] The P−O and P−C bonds in DMMP are less reactive than P−F bonds in actual nerve agents. Therefore, the use of DMMP can provide a good measure for monitoring the effectiveness of methods to degrade CWAs.[2]

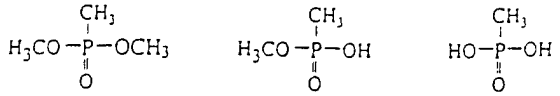

Figure 1. Structures of dimethyl methylphosphonate (DMMP), methyl methylphosphonate (MMP), and methylphosphonic acid (MPA).

An important area recently investigated for CWA decomposition is catalytic oxidation using metals and metal oxides.[1,3−11] Early studies have examined the adsorption and reaction of DMMP vapor with surfaces of metals, including Mo(111),[3] Pt(111),[4] Pd(111),[5] and Ni(111),[5] and with metal oxides such as Al_2O_3,[7] SiO_2,[8] Fe_2O_3,[8,9,11] MgO,[11] and La_2O_3.[11] More recently, the catalytic oxidation of DMMP has been studied using Pt/Al_2O_3,[1] Pt/TiO_2/cordierite,[12] and Cu-substituted hydroxyapatite[6] using temperatures between 150 and 500

* To whom correspondence should be addressed.
† Department of Chemistry, University of Connecticut.
‡ Department of Chemical Engineering, University of Connecticut.
§ Institute of Materials Science, University of Connecticut.
∥ United Technologies Research Center.

(1) Tzou, T. Z.; Weller, S. W. *J. Catal.* **1994**, *146*, 370−374.
(2) O'Shea, K. E.; Beightol, S.; Garcia, I.; Aguilar, M.; Kalen, D. V.; Cooper, W. J. *J. Photochem. Photobiol. A: Chem.* **1997**, *107*, 221−226.
(3) Smentkowski, V. S.; Hagans, P.; Yates, J. T., Jr. *J. Phys. Chem.* **1988**, *92*, 6351−6357.
(4) Henderson, M. A.; White, J. M. *J. Am. Chem. Soc.* **1988**, *110*, 6939−6947.
(5) Guo, X.; Yoshinobu, J.; Yates, J. T., Jr. *J. Phys. Chem.* **1990**, *94*, 6839−6842.
(6) Lee, K. W.; Houalla, M.; Hercules, D. M.; Hall, W. K. *J. Catal.* **994**, *145*, 223−231.
(7) Templeton, M. K.; Weinberg, W. H. *J. Am. Chem. Soc.* **1985**, *107*, 97−108.
(8) Henderson, M. A.; Jin, T.; White, J. M. *J. Phys. Chem.* **1986**, *90*, 4607−4611.
(9) Hedge, R. M.; White, J. M. *Appl. Surf. Sci.* **1987**, *28*, 1−10.
(10) Ekerdt, J. G.; Klabunde, K. J.; Shapley, J. R.; White, J. M.; J. T., Jr. *J. Phys. Chem.* **1988**, *92*, 6182−6188.
(11) Mitchell, M. B.; Sheinker, V. N.; Mintz, E. A. *J. Phys. Chem. B.* **1997**, *101*, 11192−11203.

10.1021/cm980664w CCC: $18.00
Published on Web 06/11/1999

°C. In these recent studies,[1,6,12] high DMMP conversions were observed at the beginning of the reactions, with CO_2 and H_2O as major products. Catalyst deactivation due to adsorbed phosphate species then occurs, and methanol was often observed. No P-containing products were observed in the gas phase. HPLC analyses of the spent catalysts or condensates at the ends of the reactor showed the presence of partial DMMP decomposition products, such as dimethyl phosphate, monomethyl phosphate, methyl methylphosphonate, methylphosphonic acid, and phosphoric acid.[1]

Another method currently being investigated for CWA decomposition is photocatalytic oxidation.[2,13] Oxidative photocatalysis has been shown to be effective for decomposing a wide range of toxic organic pollutants,[14] typically using TiO_2. The advantages of this technique are that benign products such as CO_2 and H_2O can be produced, and high temperatures can be avoided. Another advantage of using photocatalysis is that it may be possible to utilize solar energy for reactions.

Many researchers have investigated the photocatalytic decomposition of organophosphorus compounds,[15-17] with several studies examining the photocatalytic decomposition of DMMP.[2,13] In these studies, DMMP was photocatalytically decomposed in aqueous suspensions of TiO_2. Major products included phosphoric acid and CO_2, with intermediates such as methylphosphonic acid, formic acid, and formaldehyde being observed. The researchers proposed that DMMP is degraded through hydroxyl radical-mediated pathways.[2] Recently, the gas-phase photocatalytic decomposition of DMMP was studied over TiO_2 films.[22] In this study, the major products were CO and CO_2 in the gas phase, and MPA and PO_4^{3-} on the catalyst. Deactivation was observed due to the buildup of the P-containing species on the catalyst.[22]

Our research group has been interested in heterogeneous photocatalytic oxidation reactions using manganese oxide catalysts.[18-20] Several gas-solid reactions have been studied including the oxidation of 2-propanol to acetone,[18] and the total oxidation of methyl halides to CO_2.[19] The best catalysts were found to be mixed-valent amorphous manganese oxides (AMO), prepared by the reduction of $KMnO_4$ with oxalic acid.[18-20] The high photocatalytic activity of AMO is due to the ease with which lattice oxygen is readily desorbed.[20] In this work, we have examined gaseous reactions of DMMP over AMO in air. Emphasis has been placed on determining reaction products, examining the role of light, and studying catalyst deactivation. Finally, a mechanism is proposed to explain the interaction of DMMP with AMO.

II. Experimental Section

A. Preparation of Materials. AMO was prepared by a redox reaction involving the reduction of $KMnO_4$ with oxalic acid. A solution containing 1.58 g of $KMnO_4$ (Aldrich, Milwaukee, Wis.) in 100 mL of distilled deionized water (DDW) was mixed with a solution containing 2.26 g of oxalic acid (Fisher, Fair Lawn, NJ) in 100 mL of DDW. The solution was allowed to mix for several hours, which then yielded a dark brownish-black precipitate. The solid was filtered and washed with DDW several times and then dried in an oven at 110 °C overnight. Prior to catalytic reactions, the AMO was ground using a mortar and pestle. DMMP was purchased from Aldrich and was used without further purification.

B. Catalytic Studies. A schematic diagram for the heterogeneous photocatalytic reactor system is shown in Figure 2. A 1000-W Xe arc lamp (Kratos, Schoeffel Instruments, model LPS 255HR Power Supply and LH 151 N lamp housing, Westwood, NJ) was used as the light source. No filters were used; therefore, radiation from the lamp spanned over the entire ultraviolet and visible range (~200–800 nm). A water bottle was placed between the light source and the reactor to remove heat and infrared radiation. Air was used as the oxidant and was passed through a bubbler containing liquid DMMP, which was kept in a water bath at 25 °C. The flow rate of air was 30 mL/min. Under these conditions, the inlet DMMP concentration is ~0.14 mol %. The gas was then passed through a stainless steel reactor containing a thin layer (50 mg) of catalyst on a Gelman Sciences glass fiber filter. The reactor temperature was kept at 40 °C, and the outlet lines were heated to 110 °C to prevent condensation of DMMP and other products.

Temperature measurements made inside the reactor indicate that the lamp causes the temperature to increase to 70 °C at the surface of AMO. These measurements were made by loading AMO into the photoreactor. A small hole was made in the glass fiber filter. A narrow thermocouple wire was then directed up from the bottom of the photoreactor through the hole in the filter such that the tip was visible from the top of the reactor and surrounded by AMO.

C. GC Analyses. Reactants and products were analyzed using a Hewlett-Packard 5890 series I gas chromatograph equipped with an automatic gas-sampling valve. A Carbowax 20M capillary column with flame ionization detection was used to analyze for DMMP and methanol. CO_2 was analyzed using a GSC Gas Pro capillary column with thermal conductivity detection. Calibration curves for methanol and CO_2 were prepared from gas standards prepared in our laboratories.

D. FTIR Analyses. Fourier transform infrared (FTIR) spectroscopy (Nicolet Magna-IR 750) was used to examine surface species on the catalysts after reaction. A DTGS detector with a KBr beam splitter was used for analysis over the entire mid-IR range (4000–400 cm^{-1}). The AMO samples were pressed into KBr pellets (2.5% AMO by weight), and transmission spectra were collected.

E. Extraction Analyses of Spent AMO. Soxhlet extractions of spent AMO were performed in $CHCl_3$ and used for analysis of adsorbed DMMP on AMO. The extracts were examined using GC analyses. Aqueous extractions of AMO after DMMP reactions were used to identify methylphosphonic acid (MPA), methyl methylphosphonate (MMP) and phosphates (PO_4^{3-}). The structures of MPA and MMP are shown in Figure 1. The aqueous extracts were prepared by placing the spent AMO in H_2O and treating it with ultrasound for 10 min. The solution was filtered through 0.22 μm filters and analyzed using a Dionex DX 500 ion chromatograph (IC) equipped with a CD 20 conductivity detector and a Dionex AS4A-SC anion exchange column. The eluent used was 1.8 mM Na_2CO_3/1.7 mM $NaHCO_3$ buffer (approximate pH = 10).

(12) Hsu, C. C.; Dulcey, C. S.; Horwitz, J. S.; Lin, M. C. *J. Mol. Catal.* **1990**, *60*, 389–395.
(13) O'Shea, K. E.; Garcia, I.; Aguilar, M. *Res. Chem. Intermed.* **1997**, *23*, 4, 325–339.
(14) Linsebigler, A. L.; Guangquan, L.; J. T., Jr. *Chem. Rev.* **1995**, *95*, 735–758.
(15) Krosley, K. W.; Collard, D. M.; Adamson, J.; Fox, M. A. *J. Photochem. Photobiol. A: Chem.* **1993**, *69*, 357–360.
(16) Grätzel, C. K.; Jirousek, M.; Grätzel, M. *J. Mol. Catal.* **1990**, *60*, 375–387.
(17) Harada, K.; Hisanaga, T.; Tanaka, K. *Water Res.* **1990**, *24*, 11, 1415–1417.
(18) Cao, H.; Suib, S. L. *J. Am. Chem. Soc.* **1994**, *116*, 5334–5342.
(19) Lin, J. C.; Chen, J.; Suib, S. L.; Cutlip, M. B.; Freihaut, J. D. *J. Catal.* **1996**, *161*, 659–666.
(20) Chen, J.; Lin, J. C.; Purohit, V.; Cutlip, M. B.; Suib, S. L. *Catal. Today* **1997**, *33*, 205–214.
(21) Christol, H.; Levy, M.; Marty, C. *J. Org. Chem.* **1968**, *12*, 459–470.
(22) Obee, T. N.; Satyapal, S. *J. Photochem. Photobiol., A: Chem.* **1998**, *118*, 1, 45–51.

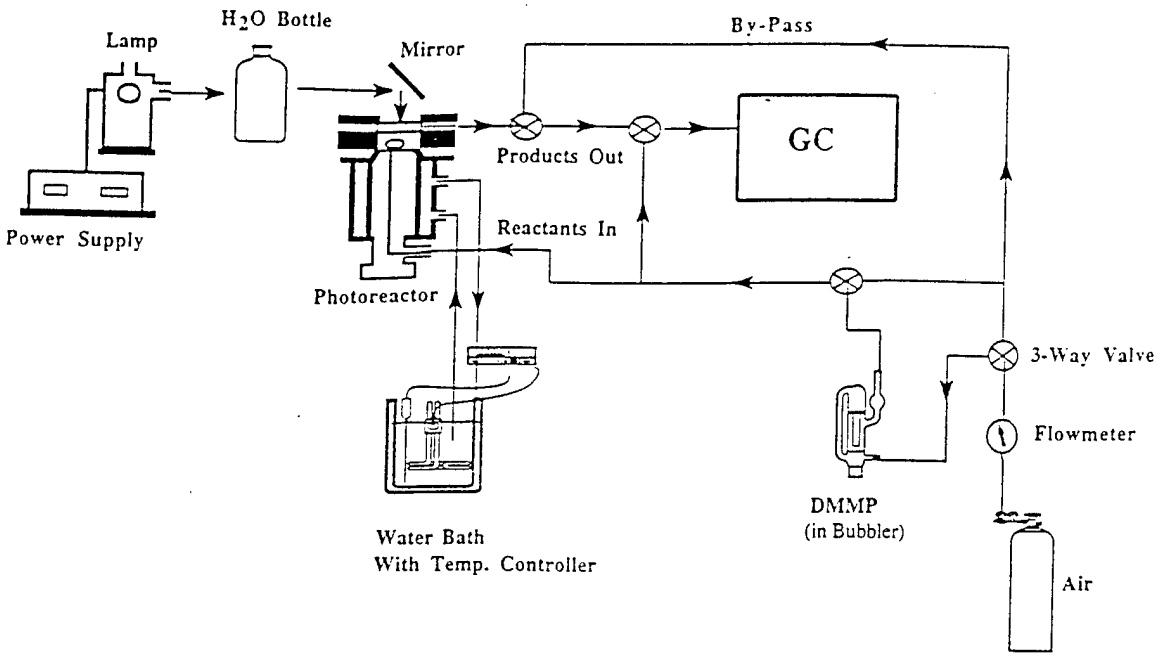

Figure 2. Experimental set-up used for photoreactions.

To confirm the presence of MPA and MMP in the IC analyses, standards were prepared and retention times were established. MPA was available commercially (Aldrich), whereas MMP needed to be synthesized in our laboratories. MMP was prepared according to literature procedures by partial hydrolysis of DMMP in aqueous NaOH solution.[7] In this procedure, 0.140 mol of DMMP was added to 150 mL of a 10% NaOH solution, and refluxed gently for 5 h. The solution was cooled slowly and acidified to pH = 2 with concentrated HCl. The solution was vacuum-distilled until a NaCl precipitate was observed in the distillation flask. The mixture was extracted several times with acetone and then filtered. The acetone extract was dried over $CaSO_4$ for several hours. The extract was refiltered and placed in a rotovap until ~15–20 mL of liquid remained. The sample was vacuum distilled, and a distillate was collected almost immediately. This distillation was necessary to remove trace amounts of acetone in the mixture. Following several more minutes of distillation, a small amount of liquid (~1 mL) was observed in the receiving flask. The liquid was identified as MMP and was confirmed by ^1H NMR studies.[21]

III. Results

A. AMO Preparation. The redox reaction between $KMnO_4$ and oxalic acid leads to the precipitation of AMO, which after drying has a composition of $K_{0.6}Mn_{0.93}O_2$.[20] The average Mn oxidation state in AMO has been determined to be 3.5–3.6, indicating that Mn exists in mixed valencies, most likely a mixture of 3^+ and 4^+, with some 2^+.[20] Powder X-ray diffraction patterns for AMO show no peaks, indicating that the material is amorphous. Pore size distribution measurements show that AMO is a porous material, having a surface area of 200 ± 10 m^2/g.[19]

Combustion analyses indicate that trace amounts of carbon (0.17%) exist in AMO. In the preparation of AMO, oxalic acid is oxidized to CO_2 and water, while the permanganate ion is reduced. Due to the vigorous nature of the reaction, some CO_2 becomes entrapped in the pores of the solid. The CO_2 may also be derived from unreacted oxalic acid remaining in the material.[18] This became apparent as CO_2 was initially detected when passing air over illuminated AMO. After a short period of time, the CO_2 would decrease. Therefore, prior to each experiment, air was passed over AMO under illumination to remove or desorb any CO_2 originating from the catalyst. After 30 min, no CO_2 was detected during photodesorption of AMO.

B. DMMP Reactions over AMO. DMMP reactions run in the absence of AMO indicate that no DMMP decomposition occurs when irradiated with light. DMMP reactions over AMO were typically run over time periods of about 5 h. Figure 3 a shows the fate of DMMP as a function of time. In the first 131 min, the reaction was performed under dark conditions. This was done because it was found that DMMP adsorbs on AMO in the dark. Therefore, it was necessary to allow the DMMP to adsorb in the dark until the surface was saturated and the inlet and outlet DMMP concentrations became equal. After this time, the lamp was turned on and the reaction was allowed to continue for another 141 min. The results show that under dark conditions, the concentration of DMMP initially decreases to ~17% of the original concentration, then climbs slowly back to the inlet concentration after 2 h. When the lamp is turned on, the DMMP concentration increases to over three times the original concentration and then quickly falls back to the original inlet concentration where it levels off. All runs were duplicated several times with fresh AMO to ensure reproducibility.

The chromatographic results using flame ionization detection also showed the presence of another peak, which was identified as methanol. Figure 3b shows the production of methanol (MeOH) as a function of time during DMMP reactions. Under dark conditions, small amounts of MeOH were produced, starting after 40 min of reaction. The average MeOH concentration during this portion of the reaction was ~1.2×10^{-3} mol %. When the lamp was switched on, the MeOH concentration increased dramatically to 3.33×10^{-2} mol %. The MeOH concentration then quickly decreased to 5.0×10^{-3} mol %, where it slowly leveled off.

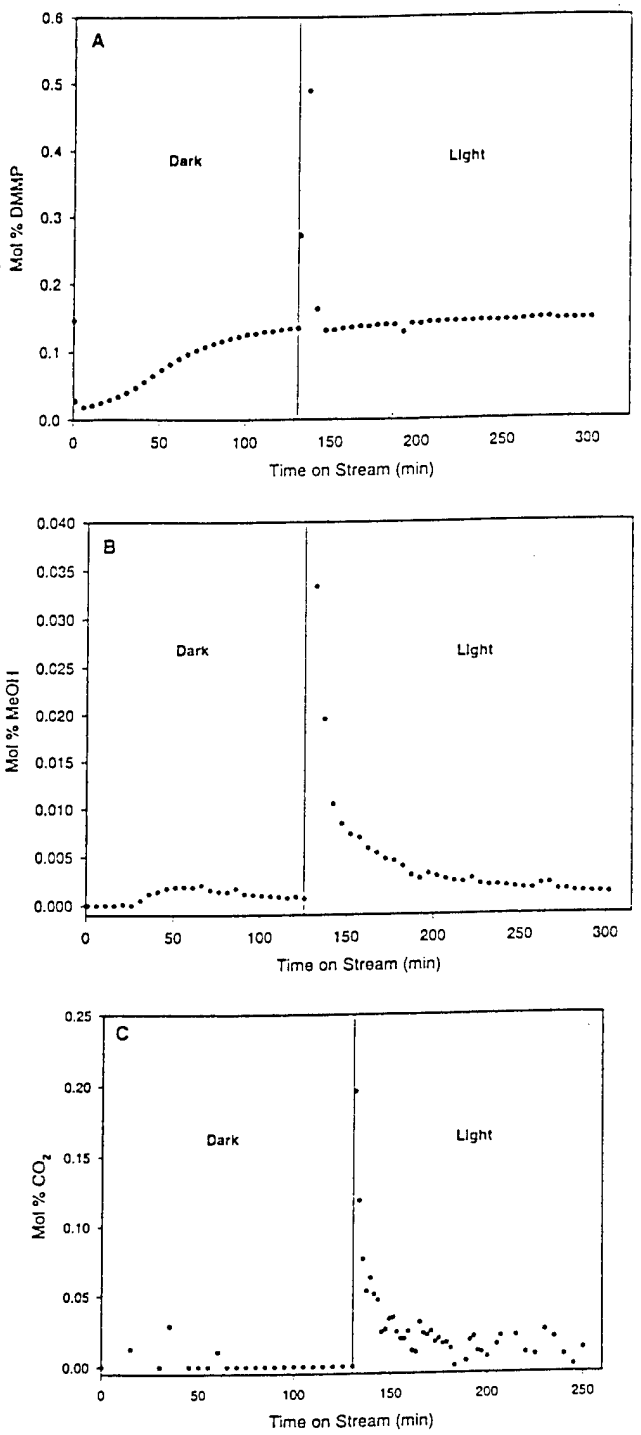

Figure 3. (a) Fate of DMMP vs time over AMO in photoreactions, (b) production of MEOH vs time over AMO in photoreactions, and (c) production of CO_2 vs time over AMO in photoreactions. Reaction conditions: 50 mg AMO, air flow rate = 30 mL/min, lamp power = 450 W.

Another product that formed during the DMMP reactions was CO_2. Figure 3c shows the formation of CO_2 during DMMP reactions. We do not see evidence of CO_2 formation under dark conditions. Some CO_2 peaks were observed toward the beginning of the reaction; presumably from noise or trace amounts of CO_2 remaining in the AMO. After the light was turned on there was a large increase in the CO_2 concentration, corresponding to 0.196 mol %. The concentration of CO_2 then quickly dropped to 0.017 mol %, where it remained fairly steady. At these low CO_2 concentrations, the analysis becomes somewhat difficult as the detection limit is approached.

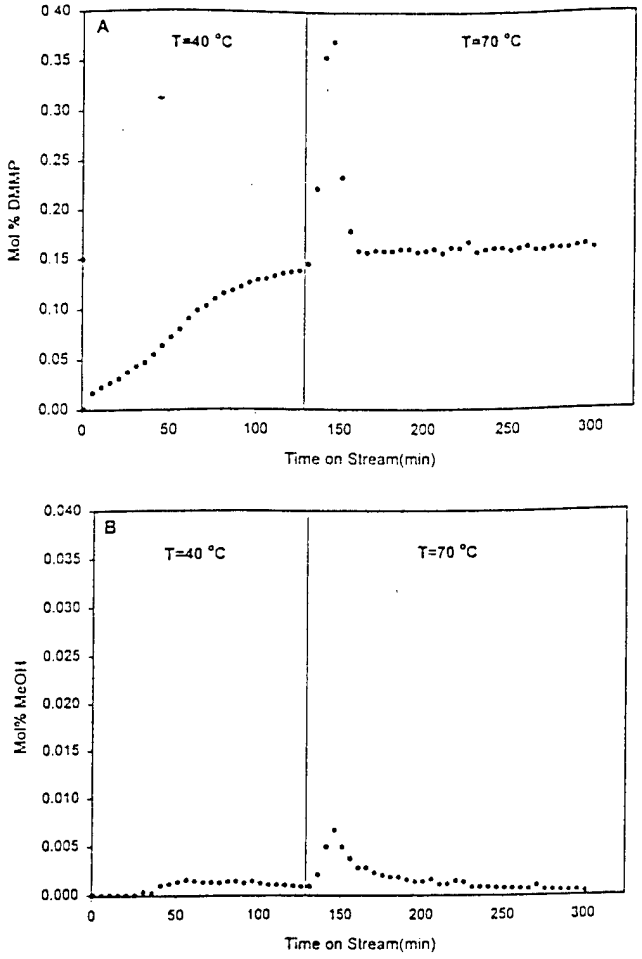

Figure 4. (a) Fate of DMMP vs time over AMO in thermal studies and (b) production of MeOH vs time over AMO in thermal studies. Reaction conditions: 50 mg AMO, air flow rate = 30 mL/min, 0−131 min = dark 40 °C, 132−272 min = dark, 70 °C.

C. Temperature Effects. Temperature measurements made inside the photoreactor indicate that light causes the temperature at the surface of AMO to increase to 70 °C. Since it is known that DMMP can decompose at high temperatures over metal oxides, experiments were performed under dark conditions at 70 °C to determine the thermal effects from light. In these experiments, the reaction was first run for 130 min in the dark at 40 °C. After this time, the temperature was increased to 70 °C (by flowing hot water through a heating/cooling jacket outside the reactor). The reaction was allowed to continue for several hours in the dark. The results for these experiments are shown in Figure 4, parts a and b. The fate of DMMP shows a similar trend to results from the photoreaction. However, as can be seen in Figure 4b, considerably less MeOH was produced in thermal reactions (max [MeOH] = 7.0×10^{-3} mol %). Under these conditions, no CO_2 was observed in thermal reactions. Turnover rates for DMMP reactions over AMO are listed in Table 1.

D. Regeneration of AMO. After several reactions with DMMP, AMO was collected (~90 mg) and placed in 100 mL of DDW and stirred for ~1 h. The sample was filtered and washed with DDW several times. The AMO sample was dried overnight in air at 110 °C, and

Table 1. Turnover Rates for DMMP Reactions over AMO

reaction	turnover rates*
dark, T = 40 °C (131 min)	1.19×10^{-3}
dark, T = 70 °C (141 min)	3.67×10^{-2}
dark, T = 40 °C (131 min)	1.20×10^{-3}
dark, T = 70 °C (141 min)	2.62×10^{-3}

*Turnover rate = (mol MeOH + mol CO_2)/mol Mn)(h). Reaction conditions are given in Figures 3 and 4.

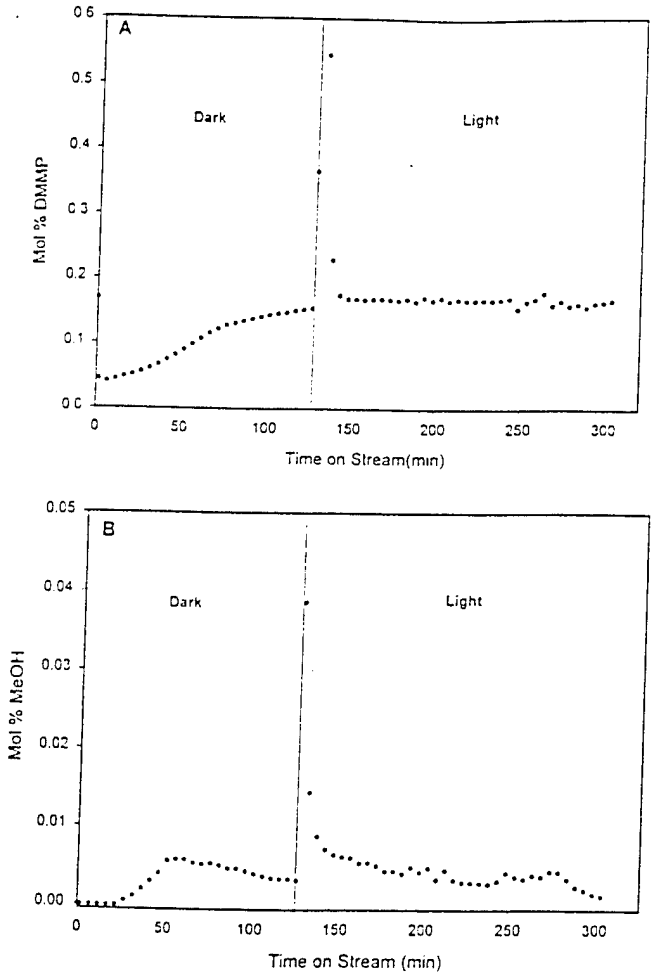

Figure 5. (a) Time course of DMMP in AMO regeneration studies and (b) production of MeOH vs time in AMO regeneration studies. Reaction conditions: 50 mg AMO, air flow rate = 30 mL/min, lamp power = 450 W.

the following day was retested as a catalyst in reactions of DMMP. Only DMMP and MeOH were analyzed in these experiments. Figure 5a shows the fate of DMMP during the reaction using regenerated AMO. This result is similar to that obtained when using fresh AMO. At the beginning of the reaction under dark conditions, the DMMP concentration decreases, although not as dramatically as in fresh AMO samples. The DMMP concentration then slowly increases to the inlet level. When the lamp was turned on, the DMMP concentration increases significantly as with fresh AMO and then levels off after several hours to concentrations near the inlet concentration.

Figure 5b shows the production of MeOH as a function of time in the regeneration experiments. The formation of MeOH also follows similar trends as fresh AMO. Under dark conditions, small amounts of MeOH (3.1×10^{-3} mol %) are formed, starting after 30 min. The MeOH concentration decreases slightly until the

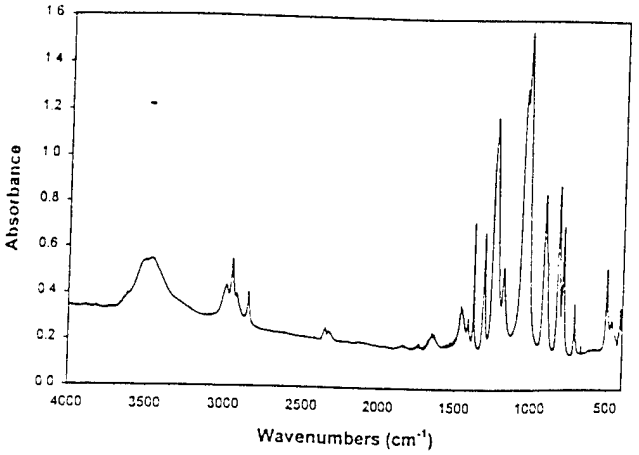

Figure 6. IR spectrum of liquid DMMP.

Table 2. IR Frequencies and Assignments for DMMP and Adsorbed DMMP on AMO after Reactions

	IR frequencies (cm^{-1})		
vibrational mode[a]	liquid DMMP	AMO dark reaction	AMO dark and light reaction
ν_a (CH_3P)	2997	2988 (0.002)	2988 (0.002)
ν_a (CH_3O)	2956	2956 (0.004)	2949 (0.002)
ν_s (CH_3P)	2930	2923 (0.003)	2926 (0.002)
ν_s (CH_3O)	2854	2852 (0.003)	2847 (0.002)
δ_s (CH_3P)	2997	2988 (0.002)	2988 (0.002)
ν (P=O)	1250	1225 (0.039)	1179 (0.035)
ρ (CH_3O)	1189	1184 (0.029)	1179 (0.035)
ν (CO)	1062	–	1052 (0.099)
ν (CO)	1036	1035 (0.147)	–
ρ (CH_3P)	914	917 (0.027)	898 (0.023)
ν (PO_2)	820	828 (0.022)	–
ν (PO_2)	789	793 (0.017)	797 (0.014)
ν (PC)	711	–	–

[a] Values for vibrational modes taken from Ref 11. ν = stretch, δ = deformation, ρ = rock. a = antisymmetric, s = symmetric. Numbers in parentheses denote absorbance units.

light is switched on. After the light is turned on, a large amount of MeOH (4.0×10^{-2} mol %) is initially observed. This corresponds to approximately the same amount of MeOH seen with fresh AMO samples. The production of MeOH then decreases as was observed with fresh AMO.

E. IR Analysis of Spent AMO. IR analyses of spent AMO were used to examine adsorbed DMMP species.

The IR spectrum of liquid DMMP was first measured for comparison and is shown in Figure 6. This was measured by placing a small amount of liquid DMMP onto a KBr pellet. The major peaks and their assignments are listed in Table 2. Peaks pertaining to DMMP occur between 3200 and 2600 cm^{-1} and between 1800 and 750 cm^{-1}. The higher frequency peaks are due to methyl group stretching vibrations, while the latter are due to C—O, C—P, and P=O stretching vibrations and methyl deformation vibrations.[11] Extra peaks occurring between 2300 and 2400 cm^{-1} are due to atmospheric CO_2, while the broad peaks around 3450 cm^{-1} are probably from small amounts of methanol or H_2O impurities in DMMP.

After reactions with DMMP, AMO was removed from the reactor and IR spectra were collected. To compare the effects of light on the adsorbed DMMP species, some AMO was removed after reaction with DMMP in the dark only (after 130 min). In Figure 7, IR spectra are shown for (a) AMO, (b) AMO after exposure to DMMP

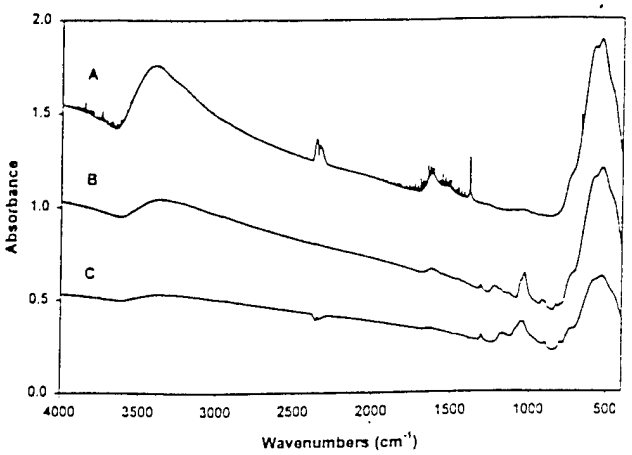

Figure 7. IR spectrum of (a) AMO, (b) AMO after reaction with DMMP in the dark, and (c) AMO after reaction with DMMP in the dark and light.

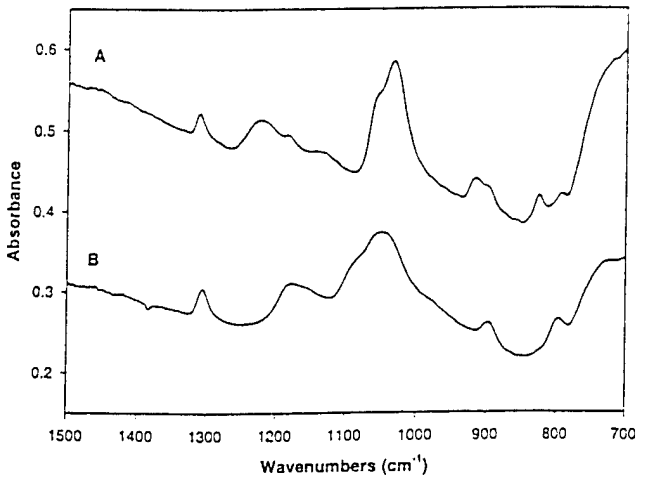

Figure 8. Lower frequency IR spectra of adsorbed DMMP species: (a) after reaction with DMMP in the dark, and (b) after reaction with AMO in the dark and light.

in the dark, and (c) AMO after exposure to DMMP in the dark and light. The assigned IR peaks for adsorbed DMMP species on AMO are given in Table 2. The IR spectrum of AMO shows an intense, broad peak centered around 500 cm^{-1}, which is due to Mn−O vibrations. Peaks between 1400 and 1800 cm^{-1}, and the broad peak at 3300 cm^{-1} are due to O−H vibrations, caused by adsorbed H_2O and hydroxyl groups on the AMO surface. Peaks are also observed between 2300 and 2500 cm^{-1}, which are due to atmospheric CO_2. The sharp peak at 1385 cm^{-1} is believed to be from an impurity in KBr.

The IR spectra of AMO after DMMP reactions in Figure 7 (parts b and c) both show the presence of many peaks associated with adsorbed DMMP. The most intense peaks occur at the lower frequencies (1800−750 cm^{-1}), while less intense peaks are observed at the higher frequencies (3200−2600 cm^{-1}). In addition, peaks caused by O−H vibrations are drastically reduced after reaction with DMMP. To see more detail, the lower frequency portion of the IR spectra are shown for AMO after reactions with DMMP in Figure 8. After dark reactions (part a), peaks can be seen at 1312, 1225, 1184, 1035, 917, 828, and 793 cm^{-1}. In the IR spectra of AMO taken after reactions done in the light (part b), similar peaks are observed; however, many of the peaks shift

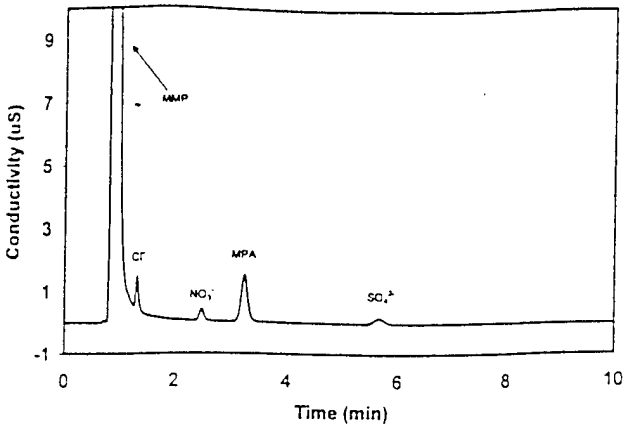

Figure 9. Ion chromatograph of an aqueous extract of AMO after reaction with DMMP in dark and light.

Table 3. Amount of MMP and MPA Produced During DMMP Decomposition Reactions

	reaction (mg/g)	
	MMP	MPA
dark (131 min)	26.54	0.10
dark (131 min) + light (141 min)	67.88	6.22
dark (272 min)	28.84	0.14

in frequency. In part b, peaks are observed at 1307, 1179, 1052, 898, and 797 cm^{-1}.

The higher frequency portion of the IR spectra of AMO after reactions with DMMP indicate that peaks appear much weaker in intensity than those of the lower frequency bands. Since these peaks are much weaker, the analysis becomes somewhat difficult. After dark reaction with DMMP, peaks are observed at 2988, 2956, 2923, and 2852 cm^{-1}. After reaction with light, similar peaks are observed; however, slight shifts to lower energies are noted, especially for CH_3O stretching frequencies.

F. Soxhlet and H_2O Extractions of Spent AMO. Soxhlet extractions in $CHCl_3$ of spent AMO after reactions in the dark and light showed the presence of DMMP, indicating that some DMMP is adsorbed molecularly. No attempt was made to quantify these data. A comparison was made between aqueous extracts of AMO after reactions with DMMP in the dark only, and with AMO after reaction in the dark and light. In Figure 9, an ion chromatogram is shown for an extract of AMO taken after reaction in dark and light. The IC analyses showed one major peak, identified as methyl methylphosphonate (MMP). A smaller peak was observed, which was identified as methylphosphonic acid (MPA). Additionally, small impurities from Cl^-, NO_3^-, and SO_4^{2-} were also observed. The IC results indicated that AMO extracts taken after dark and light reactions contained more MMP and MPA than extracts taken after dark reactions. Table 3 lists the amounts of MMP and MPA produced in DMMP decomposition reactions. To confirm that MMP and MPA are from DMMP and AMO, blank experiments were performed by treating DMMP with ultrasound and examining the products by IC. In these experiments, no MMP or MPA were observed, verifying that these products are from the decomposition of DMMP over AMO. No PO_4^{3-} was observed, indicative of incomplete decomposition of DMMP, MMP, and MPA.

IV. Discussion

A. Catalytic Results. The results from the DMMP reactions shown in Figure 3a indicate that there is a strong interaction between DMMP and AMO. Under dark conditions, DMMP is strongly adsorbed on the AMO surface. When irradiated with light, large amounts of DMMP are desorbed from the surface. This was apparent from the GC results as the DMMP concentration initially increased to three times the inlet concentration. Additionally, a condensate was observed to form on the inside of the quartz window of the reactor immediately following irradiation; presumably desorbed DMMP. These results suggest that a considerable amount of DMMP is molecularly adsorbed onto AMO and is desorbed immediately following irradiation. Since the vapor pressure of DMMP is extremely low (1.05 Torr), adsorption of DMMP on the AMO surface is favorable, especially at the low temperatures used in these reactions.

The results from Figure 3, parts b and c, show that DMMP reacts over AMO to form MeOH and CO_2. This indicates that in addition to molecular adsorption, some DMMP is adsorbed on AMO, followed by reaction to form products. The results from thermal decomposition reactions of DMMP over AMO (Figure 4, parts a and b) indicate that some thermal decomposition occurs. The turnover rate for the thermal reaction is an order of magnitude less than that for the photoreaction (see Table 1), suggesting that there is photoinduced decomposition of DMMP. The high activity initially observed after irradiation is immediately followed by fast deactivation. Under these conditions, no steady-state conversion was observed. The turnover rates for these reactions are quite low, suggesting that DMMP decomposition over AMO is stoichiometric and not catalytic.

We believe that these reactions are photoinitiated and that the initial activity is due to a photoevent. Additional thermal experiments carried out at temperatures which were measured during in situ irradiation (70 °C) showed significantly less (~8% photoproducts) product formation than during photolysis experiments. Such temperature measurements are consistent with previous studies using the same reactor in studies of decomposition of CH_3Br and oxidation of 2-proponol.[18-20] In both of these other photoreactions, there was clearly some but significantly less thermal conversion than photoconversion. A significant difference here, in the case of DMMP decomposition, is that deactivation and poisoning of the AMO catalyst is severe. We are currently devising ways to avoid such deactivation.

In catalytic oxidation studies of DMMP over metal oxides, strong deactivation is commonly observed.[1,6,12] A major concern in gas-phase catalytic studies of organophosphorus compounds over solids, is that poisoning of catalyst surfaces by PO_x species is favored, especially at lower temperatures. The total oxidation of DMMP can be represented by[6]

$$CH_3(CH_3O)_2PO + (x + 15)/2O_2 \rightarrow 3CO_2 + {}^3/_2\,H_2O + PO_x \quad (1)$$

In the total oxidation of DMMP, PO_x species cannot be removed from the catalyst unless temperatures >350 °C are used. This is because the most favored gaseous phosphorus oxide species (P_2O_5) has a sublimation point of around 350 °C.[6] In addition, the reaction of PO_x with H_2O can lead to the formation of phosphoric acid (i.e., H_3PO_4), which may also contribute to catalyst poisoning.

The results from the regeneration studies suggest that by washing spent AMO with H_2O, much of the phosphorus species can be removed. This is evident from Figure 4, parts a and b, as DMMP and MeOH plots of regenerated AMO showed similar trends as fresh AMO (Figure 3, parts a and b). Regeneration by washing TiO_2 after reaction with DMMP has also been shown to be successful.[22] In aqueous photocatalytic oxidations of DMMP over TiO_2, high conversion to H_3PO_4 was observed for several days.[13] These results indicate that H_2O may be very important in photocatalytic oxidations of DMMP over solids. This most likely occurs because H_3PO_4 and other organophosphates are soluble in H_2O, and water may help in desorbing adsorbed species from the catalysts, avoiding poisoning. Another advantage that H_2O has in photocatalytic oxidations is that reactive hydroxyl radicals are generated by photooxidation of H_2O. The hydroxyl radicals are often strong oxidants and are important in the total oxidation of many organic compounds.[13]

In our work, we have examined the effect of adding H_2O in the reaction. Experiments were performed by passing air through a bubbler containing H_2O and then mixing it with DMMP before the reactor. The results of these experiments showed that approximately the same amount of MeOH was produced compared with DMMP only reactions. These experiments suggest that a hydroxyl radical attack is not the predominant mechanism.

B. IR Analyses. The IR spectrum of AMO before DMMP reactions (Figure 7a) indicates that the AMO surface is hydroxylated. After reactions with DMMP (Figure 7, parts b and c), there is a large decrease in O−H and H_2O peaks, suggesting that DMMP either reacts with or displaces surface O−H groups on AMO. Previous IR studies have shown that photolysis of AMO can also remove H_2O from the surface.[18]

The results from the IR analyses of spent AMO (Figures 7b,c and 8 and Table 2) show the presence of many DMMP peaks. Many of these peaks are shifted toward lower energies. This is often indicative of bond weakening of adsorbed species on solids. The most pronounced shift is observed for the P=O vibration. In liquid DMMP, this peak appears at 1250 cm^{-1}. After reaction in the dark, the peak shifts to 1225 cm^{-1} and after reaction in the dark and light to 1179 cm^{-1}. This is strong evidence that the P=O moiety is involved in bonding to the AMO surface. Similar observations were recently observed in DMMP adsorption studies over Al_2O_3, MgO, and La_2O_3.[11] The interaction of P=O with Mn is consistent with a Lewis acid/base type adsorption mechanism. The phosphoryl oxygen is electron-rich,[7] and can act as a Lewis base, which can interact with Lewis acid sites on AMO (i.e. Mn^{3+}, Mn^{4+}). This leads to the formation of Mn−O=P bonds, which likely weaken the P=O bonds, consistent with the IR data. While this conclusion explains how the peak shifts from 1250 to 1225 cm^{-1}, it is not quite clear how light results in a further shift to 1179 cm^{-1}. Perhaps in light, the

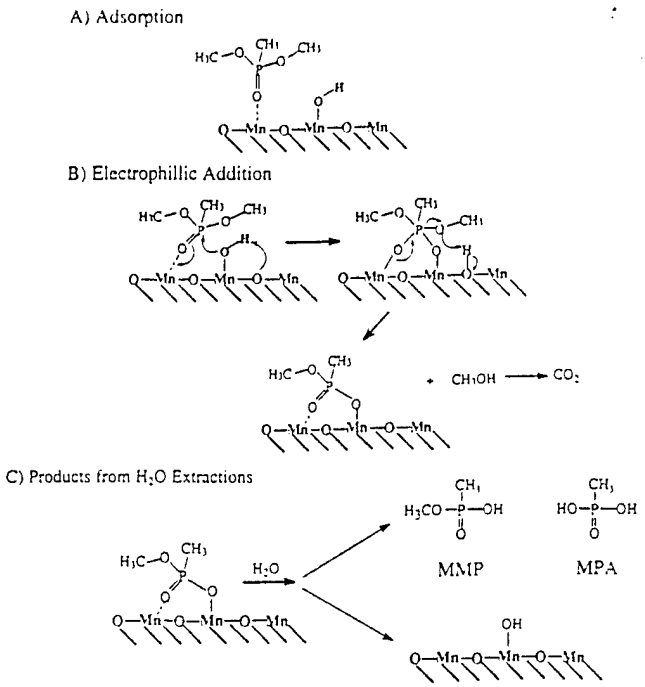

Figure 10. Scheme showing DMMP reaction mechanism on AMO surface.

phosphonate species orients differently, in a weaker interaction.

The IR spectra of Figure 8 indicate that the C–O stretching vibrations at 1062 and 1036 cm^{-1} become weaker and broader after reaction with DMMP in the light. This is consistent with the loss of methoxy groups (i.e., formation of MeOH). The peak at 1317 cm^{-1} corresponds to the CH_3P deformation. No intensity change was observed after DMMP reactions, suggesting that the P–CH_3 bond stays intact. However, this peak shifts slightly toward lower frequencies (10 cm^{-1}) after reaction in light, suggesting some weakening. The P–C stretch at 711 cm^{-1} cannot be analyzed in these studies due to interference from Mn–O peaks. Therefore, from the IR data, it is difficult to determine with certainty if P–CH_3 bonds are broken.

The peaks corresponding to PO_2 stretching vibrations at 820 and 789 cm^{-1} show several changes after DMMP reactions. After dark reactions with DMMP, the peak at 820 cm^{-1} shifts to 828 cm^{-1} and disappears after light reaction. The peak at 789 cm^{-1} shifts to higher energies after reaction with DMMP. These results suggest the formation of a new adsorbed species; perhaps a different PO_2 mode corresponding to the loss of methoxy groups (i.e., adsorbed methyl methylphosphonate).

C. Extraction Analyses and Mechanism. The Soxhlet extractions of AMO in $CHCl_3$ after reaction indicate that some DMMP is adsorbed molecularly or nondissociatively; however, H_2O extractions of spent AMO show that adsorbed DMMP reacts to form MMP and smaller amounts of MPA (Table 3). At the suggestion of a reviewer, an additional experiment was performed where the DMMP reaction was run over AMO in the dark for 272 min. These results show that roughly the same amount of MMP and MPA are produced as compared to dark only reactions after 131 min. The formation of MMP and MPA are consistent with the GC and IR data. A possible mechanism is shown in Figure 10. DMMP is first bonded to AMO via the phosphoryl oxygen. The second step involves electrophilic attack by the AMO surface on DMMP, leading to the loss of a methoxy group. This probably occurs by abstraction of hydrogen from AMO surface hydroxyl groups, which results in the evolution of MeOH and the formation of an adsorbed methyl methylphosphonate species. This species is then hydrolyzed in H_2O to form MMP and some MPA. This mechanism is similar to those observed in DMMP adsorption and decomposition studies by Mitchell et al. over Al_2O_3, MgO, and La_2O_3.[11]

Another possible mechanism involves superoxide anion radicals ($O_2^{\bullet-}$), which can form from the photoreduction of O_2. Superoxide anion radicals may react with DMMP as a nucleophile, causing hydrolysis and loss of a MeOH group. Further photoreactions were done in N_2, which showed that approximately the same amount of MeOH is produced in both cases. Since MeOH is produced in the absence of O_2, this suggests that a superoxide anion radical mechanism is not occurring. However, since AMO is known to release O_2 during photolysis, it cannot be completely ruled out that superoxide anion radicals do not form.

A reviewer has suggested that the formation of MeOH in the dark may be due to acid-catalyzed surface hydrolysis. This may be the case, since in the preparation of AMO, an acidic precursor is used (oxalic acid). It is therefore possible that the AMO surface is protonated. Several experiments were performed to examine this possibility. In one experiment, an unwashed sample of AMO was tested. It would be expected that an unwashed sample of AMO would be more acidic than washed samples of AMO. Another experiment was done using H^+–AMO, prepared by exchanging K^+ in AMO with NH_4^+. Following ion exchange, the sample was heated to evolve NH_3 leaving H^+–AMO.

In both cases, the enhancement of acidity of AMO to generate Brønsted sites led to materials that produced similar amounts of methanol. These data are somewhat inconclusive, since the number of acid sites was increased, but we have little information on the exact numbers, amounts, strengths, or types of sites introduced with this indirect method. In addition, the originally present acid sites are very likely still present and could still potentially give rise to methanol formation. We are unsure about the mechanism of methanol formation in the dark. At this point Brønsted acid, Lewis acid, or base sites cannot be ruled out.

The CO_2 formed in these reactions most likely comes from the photooxidation of methoxy groups of DMMP and possibly from the photooxidation of MeOH. Manganese oxide supported Al_2O_3 has been shown to be able to photooxidize MeOH to CO_2.[23] An experiment was done to determine if MeOH can be photooxidized to CO_2 over AMO. In this experiment, a small amount of liquid MeOH was placed on AMO, and then put into the photoreactor. When the sample was irradiated with light and air was passed over it, large amounts of CO_2 were observed. In thermal reactions done in the dark at 70 °C, no CO_2 was observed, suggesting that light is necessary for CO_2 formation. Since no phosphoric acid was detected in the AMO extracts, more conclusive

(23) Okzan, U. S.; Kueller, R. F.; Moctezuma, E. *Ind. Eng. Chem. Res.* **1990**, *29*, 1136–1142.

evidence is provided suggesting that no $P-CH_3$ oxidation is occurring.

V. Conclusions

To the best of our knowledge, this is the first report of DMMP decomposition reactions over manganese oxide materials. DMMP was found to strongly adsorb to AMO, with both physi- and chemisorption occurring. Initial irradiation of adsorbed DMMP on AMO shows that DMMP reacts to form CO_2 and MeOH. The CO_2 produced comes from the photooxidation of methoxy groups and not from oxidation of $P-CH_3$. The decomposition reaction occurs due to a combination of thermal and photoinduced effects. The strong adsorption of DMMP on the AMO surface leads to severe poisoning. Several products accumulate on the AMO surface, including MMP and MPA, which most likely contribute to the catalyst poisoning.

In the future we will try to improve the activity of gas- phase photoassisted DMMP decomposition reactions. One way in which this may be accomplished is by optimizing the catalyst synthesis. We are currently examining the addition of dopants, changing reactant concentrations, and the use of different reducing agents. To better understand AMO deactivation by DMMP and to improve conversion efficiencies, we are currently investigating thermal reactions (i.e., >70 °C) of DMMP over AMO.

Acknowledgment. We thank the U.S. Army and United Technologies Research Center, East Hartford, CT, for support of this work. This work was supported by the U.S. Army Research Office, under contract DAAH04-96-C-0067. The authors thank Dr. Jie Chen and Lisa Washmon for preliminary work done on this project. The authors also thank Dimitri Gumerov for collecting portions of the IC data.

CM980664W